Using Palomar Gattini-IR to study Core-collapse Supernovae and Probe their Red Supergiant Progenitors

Thesis by
Gokul Prem Srinivasaragavan

In Partial Fulfillment of the Requirements for the
Degree of
Bachelor of Science in Astrophysics

Caltech

CALIFORNIA INSTITUTE OF TECHNOLOGY
Pasadena, California

2021
Defended [June 4, 2021]

ACKNOWLEDGEMENTS

This thesis truly would not have been possible without the help and support from some amazing individuals, whom I would like to thank:

To begin with, I am grateful to my advisor, Mansi Kasliwal. Mansi's enthusiasm for hunting, observing, and understanding astrophysical transients inspired me to delve deeper into the field of transient astronomy, which has ended up becoming an avenue of research that I am actively looking to make strides in during graduate school. But though Mansi is incredible as a research advisor from an academic point of view, it pales in comparison to how incredible she is as a human being. Your kindness, empathy, and genuine support throughout the past year and a half, a time period of my life that has been very tough on a personal level, has been one of the biggest reasons I have been able to succeed in my research endeavors. I am so lucky to have such an incredible person to look up to as a role model as my academic career moves forward.

I am grateful to David Hsieh, my Physics 1c Professor from Freshman year. David taught the first physics class I took at Caltech on grades, and I struggled heavily during the class, despite an immense amount of effort and hard work put into it. After earning a C in the course, I seriously doubted my abilities and whether I could truly successfully pursue a career in astronomy and physics. At one of the lowest moments of my academic life, I turned to David for advice, and his kind and encouraging words inspired me to continue pursuing my passions, which I will be forever grateful to him for. Thank you for being an incredible mentor, you are truly a role model for the type of Professor I hope to be one day.

I am grateful to Maria Dainotti, my research advisor from the summer of 2019 through the summer of 2020. Maria took me under her wing when I was fresh out of sophomore year and an ACL surgery, and the first summer I spent working with her at Stanford was truly a career-changing experience. Thank you for introducing me to the amazing field of high-energy astrophysics, another field that I hope to make strides in during graduate school, and for giving me the opportunity to first-author my first ever paper. Your support and patience over the past two years are a huge reason why I am where I am today.

I am grateful to Oliver Eslinger, the Head Men's Basketball Coach at Caltech. Thank you for being one of the most caring, empathetic coaches that I have ever had. My

years playing basketball at Caltech, even despite missing a year due to injury and another due to the pandemic, have been the best years of basketball of my life. Thank you for supporting my dreams both on and off the court, and I hope I made good on the promises I made to you when you recruited me about how I would help orchestrate change in Caltech's hoop culture. I cannot wait to keep following the program in the future, and see you eventually bring home that first conference championship.

To the PGIR team. Thank you so much for taking me under your wing and teaching me the ins and outs of time-domain astronomy in the near-infrared. In particular, I would like to express my gratitude to Jacob Jencson, Kishalay De, and Matthew Hankins for being amazing research mentors.Thank you for being incredibly patient and supportive of my research efforts. Your advice about the graduate school admissions process was also incredibly helpful and reassuring during one of the most stressful time-periods of my life, and I look forward to keeping in touch as I continue my career in astronomy. I also would like to express my gratitude to Michael Ashley, who I worked with heavily during the summer of 2020 on what eventually became Chapter 3 on this thesis. Thank you for being an incredibly supportive research mentor, and for introducing me to an incredibly interesting field of astronomy research I had no prior experience in- instrumentation.

To my closest friends. Laith Anqud; you have become nothing short of my brother over the past seven years. Thank you for being there for me for everything from hoop to science and everything in between, even when we walk ten miles around Picadelly Park in the process. Jonathan Babu; our friendship over the years is the source of so many of my happiest memories. Thank you for trusting me to help you in your physics and astronomy courses, our conversations about the universe have truly made me a better scientist. Jason Zhou; you are the true definition of what it means to be a selfless friend. Your kindness and compassion have helped me through some very trying times, and I am so grateful. Sneha Ramesh; your unconditional friendship through good times, bad times, and everything in between gave me strength to push through some of the toughest trials in my life. Thank you for being there for me through it all. Brendon Macias; you have been like a big brother to me for the past eight years. From driving six hours from Arizona to support me at my games, to talking about quantum mechanics theories in my room at Caltech, the memories we have together are unforgettable. Vinayak Kumar; you are truly one of the most amazing minds I have ever had the honor of being friends

with, that too for 16 years. Thank you for having my back since Kindergarten, and I cannot wait to see the amazing things you achieve in your academic career going forwards. Marcus Gee, Nayla Abney, and Krystin Brown; without the three of you, I honestly do not think I would be writing this thesis right now. Marcus, the memories we shared on the court will always be some of my fondest hoop memories, but bigger than that, your friendship along with Nayla's and Krystin's is what gave me the strength to push through a freshman year where I constantly doubted myself and my abilities. The memories we have made together over the past four years are ones I will cherish forever. Stephen Hei and Noah Barnes; my fellow Big Guards. I am so grateful for the bond we created over the past three years, on and off the court. Having you two by my side while we went through the trials of Caltech together meant everything to me. I cannot wait to watch you two and Marcus dominate the SCIAC next year. Jerome Seebeck; thank you for making solving physics sets and studying for finals together more fun than I ever thought was possible. You are one of the brightest people I have ever met, and I cannot wait to see the amazing things you achieve in your astronomy career. Lauren Suezaki; thank you for being a constant source of support and someone who I knew always had my back during my time at Caltech, especially on the court. I am so grateful for our friendship. Simi Bhullar; your unwavering support, kindness, and friendship during the months I have been finishing this thesis have meant so much to me. Thank you for helping me find the strength to push through the final stretch of my Caltech career. Anirudh Murugesan; I am grateful to have found another little brother through our friendship. Thank you for trusting me to give you advice about life both on and off the court, and I cannot wait to see the amazing things you do in college and beyond. Eric Hsueh and Ishan Shah; we started out as teammates in middle school, and I am forever grateful to hoop for creating brotherhoods like the one I share with you two. Thank you for being there for me and supporting me over the past eight years. Ashal Shazhad, Nickolas Nguyen, Aman Johal, and Parker Matsumoto; thank you for supporting me both as an athlete and as a scientist ever since high school. The memories we have made together are some of the funniest and fondest that I always end up thinking about during tough times.

And finally, last but definitely not least, to my amazing family. Rahul; you are the best little brother I could have ever asked for. Thank you for always bringing a smile to my face even during the toughest times, and for trusting me to be your trainer and biggest critic on the court, and your tutor off of it. I cannot wait to see the incredible things you achieve both academically and athletically in the next chapter

of your life. Amma; I can't begin to express how much you mean to me. Thank you for reassuring me through all of the tears and frustrations I have vented to you about over the past 21 years, and for being my biggest supporter on and off the court no matter what. To this day, despite all of the incredibly challenging classes and research problems I have had to tackle over the past four years, our study sessions together for elementary school math top it all. Thank you for being the most amazing mother in the entire world, and for making me the most delicious dosas for the past 21 years. Appa; there aren't enough words to talk about how much you mean to me too. Looking up to you as a role model has made me the best person I could possibly be, and your support on the court as my coach, biggest critic, and eventually my biggest fan, along with in my academic career is the singular biggest reason I am here right now writing this thesis. The smile I see on your face whenever I tell you one of my accomplishments is even more meaningful than the accomplishments themselves. I hope that this thesis makes you guys proud!

ABSTRACT

Core-collapse supernovae (CCSNe) are extremely energetic explosions that originate from the death of massive stars. CCSNe are rich astrophysical events that have an enormous amount of implications, ranging from understanding the physics of shock breakouts, to unraveling how heavy elements are produced through nucleosynthesis, to much more. The first part and bulk of this thesis is on the analysis of SN 2020qmp, a nearby Type II-P CCSNe discovered by the Palomar Gattini-IR (PGIR) survey.

SN 2020qmp displays characteristic hydrogen lines in its optical spectra, as well as a plateau in its optical lightcurve (LC), allowing us to characterize it as a Type II-P supernova. We do not detect any polarization (specifically, we find the broadband degree of polarization to be $0.14 \pm 0.26\%$, with an upper limit in 3σ of 0.78%) of the SN during the plateau phase. Through hydrodynamical LC modeling and an analysis of its nebular spectra, we estimate a progenitor mass of around 12 $M_\odot$. We find that SN 2020qmp cannot be explained by a simple circumstellar medium (CSM) interaction model, assuming a constant shock velocity and mass-loss rate in steady winds, and observations in the radio and X-rays seem to indicate possible deviations from equipartition. Finally, we find that NIR surveys are more sensitive to extincted CCSNe than optical surveys in the local universe. Specifically, we estimate that the Wide-Field Infrared Transient Explorer (WINTER) will detect around 14 CCSNe that the Zwicky Transient Facility (ZTF) will miss due to dust extinction effects in a five year time period. We encourage extensive multi-wavelength follow-up observations for all nearby CCSNe, because their detailed characterizations offer unique insights into massive star explosions.

This thesis concludes with efforts made by the PGIR team to increase the dynamic range of the detector, so that robust near-infrared LCs of Red Supergiant (RSG) candidates in our galaxy can be obtained. These LCs would be invaluable when one of these RSG candidates explodes into a CCSNe, especially combined with neutrino and gravitational wave observations, which would open an exciting new avenue of CCSNe multi-messenger studies.

TABLE OF CONTENTS

LIST OF ILLUSTRATIONS

Chapter 1

INTRODUCTION

Core-collapse supernovae (CCSNe) are some of the most energetic astrophysical phenomena in the universe, and are the result of the death of stars at least 7-9 times more massive than the Sun (Stephen J. Smartt, 2009). CCSNe have been a major topic of study from both a theoretical and observational point of view, for a variety of rich reasons.

CCSNe theoretical studies are rapidly developing and evolving, and gain more traction with every technological advance in high-performance computing. These studies usually focus on understanding the explosion mechanisms for CCSNe through creating 3D simulations ran in supercomputers. These supercomputers only recently have been able to model the most complex physical processes characteristic to the explosions, such as neutrino heating and the breaking of spherical symmetry within the explosion (Burrows et al. 2021). Theoretical studies also include the creation of supernova explosion codes (Utrobin and Chugai, 2015; Utrobin and Chugai, 2017; Morozova, Piro, and Valenti, 2017; Morozova, Piro, and Valenti, 2018; Goldberg, Bildsten, and Paxton, 2019; Martinez and Bersten, 2019), that use hydrodynamical LC modeling to generate optical LCs of CCSNe that can be used to compare to observations. From an observational point of view, different aspects of the explosion can be analyzed through various techniques. Multi-wavelength spectroscopic observations of the explosion can be utilized to analyze the elements produced in these explosions for astrochemistry purposes. These heavy elements in turn enrich the surrounding interstellar medium (ISM), which plays an important role in triggering new sites of star formation. Spectropolarimetry of the explosion can also be used to understand whether the ejecta outflow is asymmetric in order to better understand the physics of the shock breakout. Furthermore, photometric observations in the UV, optical, and infrared wavelengths and their resulting LCs can be used to study the behavior of the explosion and how it varies over time, as well as to classify the explosion to its different observational sub-classes.

However, CCSNe are important not only from the perspective of the explosions themselves, but also due to their aftermath. The remnants of CCSNe are compact objects- either neutron stars or black holes. Both these compact objects are topics

of extensive studies on their own. However, understanding the preceding CCSNe of these objects can help shed light on the black hole mass-gap - where there is an unexplained absence of 2-5 $M_\odot$ black holes in the galaxy (Özel et al., 2010) (though recently, a "unicorn" object of 2.9 $M_\odot$ that is either the largest neutron star or smallest black hole ever has been discovered; Jayasinghe et al. 2021). It has been suggested in the past that this mass-gap may be due to a step-function dependence between CCSNe red supergiant (RSG) progenitor masses and their corresponding explosion energies, that goes to zero for massive stars greater than 25 $M_\odot$ (Fryer and Kalogera, 2001). Better understanding the late stages of CCSNe explosions and the physical processes driving the formation of these compact objects is the key to uncovering why this mass-gap exists.

Finally, studying the RSG progenitor sources for CCSNe and understanding their behavior and variability near the end of their lives is incredibly important for understanding CCSNe explosion mechanisms. This is especially true from a multi-messenger perspective, as neutrinos are emitted from RSGs even before the core-collapse process starts (Arnet et al. 1989), and constitute the main source of energy of a CCSNe in the first 10 seconds directly after explosion (Bionta et al. 1987; Hirata et al. 1987; Sato Suzuki 1987). Combining neutrino observations from CCSNe along with LCs from across the electromagnetic spectrum will provide physicists and astronomers with an immense toolbox to pull from to fully understand the beforemath, during, and aftermath of CCSNe explosions. CCSNe in general are relatively common from an extragalactic perspective, as hundreds per year are usually discovered in distant galaxies (e.g. Sako et al. 2008; Leaman et al. 2011). However, observations of these distant CCSNe are not complete enough, especially from a multi-messenger perspective, to be a true direct probe into the physics driving the explosions. This is why a galactic or extremely close extragalactic CCSNe would be a game-changer, and allow for true multi-messenger studies of CCSNe, including the utilization of not only neutrino observations but also gravitational waves.

Many known RSGs that are nearing the end of their lives exist close to the Galactic center (Nakamura et al., 2016). However, the galactic center is extremely dusty, and sources in this region of the galaxy are often hidden behind huge columns of line-of-sight extinctions in optical wavelengths. This makes near-infrared (NIR) telescopes such as the Palomar Gattini-IR (PGIR; Moore and M. Kasliwal 2019) invaluable for probing both the variability of the RSG progenitor sources as well as capturing the early-time LCs of CCSNe. PGIR is a J-band (1.25 μm) (NIR) time-

domain survey at Palomar observatory that has been in commission since September 2018, and started survey operations in July 2019. PGIR has a wider area than any other existing infrared camera by more than a factor of 40, and is able to survey the entire accessible sky from Palomar observatory (15,000 square degrees) every two nights. PGIR's ability to scan nearly the entire night sky at such a low cadence as a NIR instrument makes it an incredibly useful tool for studying CCSNe and their progenitors.

The bulk of this thesis is comprised of a detailed, multi-wavelength study of SN 2020qmp, a type II-P CCSNe that was discovered by PGIR on UT 07-30-2020. This study (Chapter 2) is written from the perspective of an academic journal article, and will be submitted to the journal Astronomy & Astrophysics. The third and final chapter points towards future efforts to probe CCSNe RSG progenitors made possible due to technical instrumentation advances made in PGIR, where we implemented a new readout mode in PGIR's detector. This new readout mode made it possible to image and collect data from RSGs near the galactic center. This effort was necessary because these sources are usually bright in the NIR, and would have saturated the detector if this new readout mode was not implemented. We end the chapter and thesis with a short discussion on how this new readout mode has the potential to have important implications for CCSNe studies in the future.

Chapter 2

PGIR 20EID (SN 2020QMP): A YOUNG TYPE II-P SUPERNOVA AT 15.6 MPC DISCOVERED BY THE PALOMAR GATTINI-IR SURVEY

2.1 Introduction

Type II supernovae are hydrogen-rich core-collapse supernovae (CCSNe) that represent the fate of stars that have a minimum mass of around 7 to 9 $M_\odot$ (Stephen J. Smartt, 2009), though the maximum mass of CCSNe progenitors is a debated topic (Utrobin and Chugai, 2009; Dessart, Livne, and Waldman, 2010; A. Jerkstrand, C. Fransson, et al., 2012). The Type II class is divided observationally into many different subclasses based on their lightcurves (LCs) and spectroscopic properties, including type II-P, II-L, and II-n, and II-b (Gal-Yam, 2017). Of these, type II-P events characterized by a plateau in their optical LCs lasting about 100 days after the explosion are most common (Branch and J. Craig Wheeler, 2017).

Though Type II-P supernovae are among the most common supernova found, it is uncommon to discover extremely nearby CCSNe (only five during the past three years within 10 Mpc reported to the Transient Name Server[1]). Nearby and bright CCSNe allow us to probe many different facets of supernova physics, including obtaining high-resolution spectra for astrochemistry purposes, astrometric pinpointing of the progenitor star (Stephen J. Smartt, 2009; S. J. Smartt, 2015), analyzing the physics of the shock breakout (Rabinak and Waxman, 2011; Sapir and Waxman, 2017), understanding the polarimetry of the supernova (Voshchinnikov, 2012; Wang and J. C. Wheeler, 2008; Nagao, Maeda, and Tanaka, 2017; Nagao, Maeda, and Tanaka, 2018; Tinyanont, M. A. Millar-Blanchaer, et al., 2019a) and opening the avenue for multi-messenger follow up on the source (Nakamura et al., 2016). Furthermore, the interaction between the blast wave of CCSNe and the circumstellar or interstellar

---

[1] https://www.wis-tns.org/

medium (CSM or ISM) generates multi-wavelength emission through synchrotron radiation processes (Roger A. Chevalier, 1998). Analyzing these observations provides key insights into the progenitor star's final years of life, and allows us to probe the very late stages of stellar evolution of massive stars with high precision (Horesh, Stockdale, et al., 2013a). Furthermore, nearby SNe are ideal for multi-wavelength observations and studies.

Palomar Gattini-IR (PGIR; Moore and M. Kasliwal 2019) is a wide-field near-infrared (NIR) time-domain survey. Located at Palomar observatory, PGIR uses a telescope with an aperture of 300 mm, and a camera field of view of 25 square degrees. These specifications allow PGIR to be an untargeted survey, and the first ever in the NIR. PGIR has a median cadence of 2 days, and can image sources up to a median depth of 15.7 AB mag (K. De, Hankins, M. Kasliwal, et al., 2020) in *J*-band. As a wide and shallow infrared time domain survey, PGIR is sensitive to infrared bright transients in nearby galaxies, including events that could be missed in the optical due to large columns of line of sight extinction.

On UT 2020-07-030, PGIR made its first extragalactic discovery of a SN with its detection of PGIR 20eid (SN 2020qmp), which was spectroscopically classified as a Type II-P SN (K. De, Hankins, M. M. Kasliwal, et al., 2020). In this paper, we present the early NIR and optical lightcurves (LCs) of SN 2020qmp during its plateau phase, as well as optical and NIR spectra taken at various time epochs. We then use hydrodynamical LC modeling in order to infer the progenitor star mass and explosion energy of the SN, and follow that with analyzing its optical spectra after it has reached its nebular phase, in order to also infer the mass of its progenitor star. We also present radio data obtained from the Karl G. Jansky Very Large Array (VLA), which allowed us to infer key characteristics pertaining to the blast wave physics as well as of the late stages of the progenitor star's life. We conclude by commenting on the local CCSNe rate, and how NIR survey is well equipped to find optically obscured CCSNe in the future due to its ability to see through large columns of line of sight extinction as a near infrared survey.

The paper is organized as follows. In §2.2, we present the observations in the UV, optical, and NIR by the Neil Gehrels *Swift* Observatory (*Swift*; Gehrels et al., 2004) the Zwicky Transient Facility (*ZTF*; Masci et al., 2018), and PGIR, along with its optical and NIR spectra and radio observations. In §2.3, we present the results of the hydrodynamical LC modeling. In §2.4, we analyze the nebular spectrum of the SN and compare it with model spectra, in order to infer the zero-age main sequence

(ZAMS) progenitor mass. In §2.5, we present the analysis from the radio data, and infer various properties regarding the blast wave and progenitor star's mass loss rate, as well as possible deviations from a standard CSM interaction model. In §2.6 we describe the local CCSNe rate and show how PGIR has the ability to detect more local CCSNe than optically-based surveys up to a certain distance. Finally, in §2.7, we summarize the main conclusions of our results.

2.2 Observations of SN 2020qmp

Photometric and X-Ray Observations

PGIR 20eid was first detected in the automated image subtraction and transient detection pipeline of the PGIR survey on UT 2020-07-30, at a (RA, Dec) of (12h08m44.43s, +36:48:19.4), and at magnitude $J = 14.74 \pm 0.2$ AB mag. This source was detected as part of a filter for large amplitude transients described in (Kishalay De et al., 2021). The transient was detected on the spiral arm of galaxy UGC07125, which has a distance of 15.6 Mpc (Tully, Courtois, and Sorce, 2016), and a diameter of 21.61 kpc (de Vaucouleurs et al., 1991). Assuming this distance, the absolute magnitude of the transient upon first detection was $M = -15.7$ in J band. The latest non-detection by PGIR was on UT 2020-07-25, up to a 5σ limiting magnitude of $J = 15.1$ AB mag. The discovery location of the SN by PGIR, along with an image from the Pan-STARRS1 survey (Kaiser et al., 2002) for reference are shown in Figure 2.1.

Though PGIR made the initial discovery of the SN, the Zwicky Transient Facility (ZTF) made a detection of the SN on UT 2020-07-26 (ZTF20abotkfn). The latest non-detection by ZTF was on UT 2020-07-22, up to a limiting magnitude of $i = 19.1$ AB mag. We estimate the explosion date to be the average of the latest non-detection by ZTF and the first detection, on UT 2020-07-24. ZTF continued to make detections of the SN in the r, g, and i-bands.

Following the initial announcement of the discovery (K. De, Hankins, M. M. Kasliwal, et al., 2020), the transient was followed up by *Swift* using the Ultra-Violet Optical telescope (UVOT) and the X-ray telescope (XRT). *Swift* observed the field with the Ultraviolet/Optical Telescope (UVOT; Roming et al., 2005) between 31 July and 8 August 2020 (PI: Paraskeva). The brightness in the UVOT filters was measured with UVOT-specific tools in the HEAsoft version 6.26.1. Source counts were extracted from the images using a region of 3″. The background was estimated using a circular region with a radius of 29″ close to the SN position. The count rates
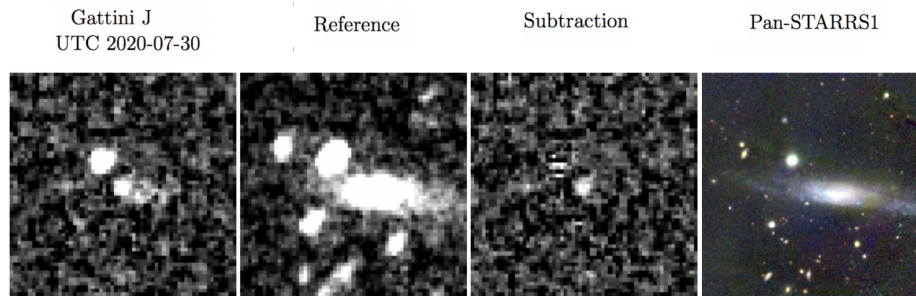
Figure 2.1: Discovery location of SN 2020qmp, containing images from the night of first detection, UT (2020-07-30) taken by PGIR. An image from the Pan-STARRS1 survey is also included as reference.

were obtained from the images using the *Swift* tool uvotsource. They were converted to magnitudes using the UVOT photometric zero points (Breeveld et al., 2011). Due to the lack of host templates, the SN flux includes the contribution from the host galaxy. All magnitudes were transformed into the AB system using Breeveld et al. (2011). The LC of the SN over a range of wavelengths is shown in Figure 2.2. We also calculated the bolometric LC of the SN (shown in §2.4), by performing a black body fit with all available filters at every photometric epoch available, and then integrating the black body to derive a luminosity. In the early-time LC during the first 20 days after explosion, we use all photometric points within one days of the day in question in our black body fits, as the early-time LC is very variable. After 20 days, we include all photometric points within four days of the day in question, and then perform black body fits for every day there are at least three different wavelength bands available.

Swift also used the onboard X-Ray Telescope (XRT; Burrows et al., 2005) in the energy range from 0.3 to 10 keV. We analyzed all data with the online-tools of the UK *Swift* team[2] that use the methods described in Evans, Beardmore, Page, Tyler, et al. (2007) and Evans, Beardmore, Page, Osborne, et al. (2009) and the software package HEASOFT[3] version 6.26.1.

Combining the four epochs taken in July/August 2020 amounts to a total XRT exposure time of 3982 s, and provides a marginal detection of $0.0014^{+0.0009}_{-0.0007}$ count s^{-1} between 0.3 and 10 keV. If we assume a power-law spectrum with a photon index

---

[2] https://www.swift.ac.uk/user_objects/
[3] https://heasarc.gsfc.nasa.gov/docs/software/heasoft/
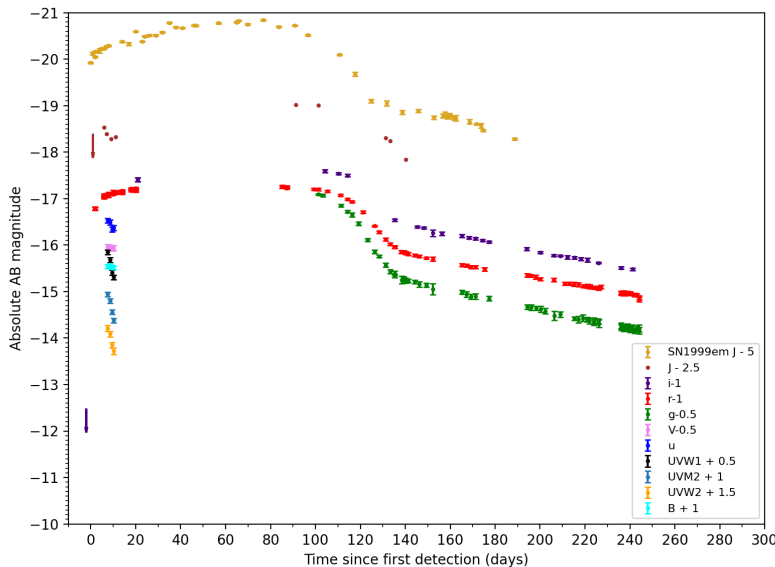
Figure 2.2: Light curve of SN 2020qmp. The light curve includes photometry points from the PGIR survey (*J*-band) as well as the *Swift* UVOT telescope (*UVW*1, *UVM*2, *UVW*2, *u* and *B* bands), and ZTF (*i*, *r* and *g* bands), as well as the LC of SN1999em in J band (Krisciunas et al., 2009).

of $\Gamma = 2$ and a Galactic hydrogen column density of 1.95×10^{20} cm^{-2} (HI4PI Collaboration et al., 2016) this corresponds to an unabsorbed 0.3–10.0 keV flux of $5.1^{+3.3}_{-2.6} \times 10^{-14}$ $erg\, cm^{-2}\, s^{-1}$. At the luminosity distance of PGIR20eid this corresponds to a luminosity of $L_X = 2 \pm 1 \times 10^{39}$ erg s^{-1} (0.3–10 keV) at an epoch of MJD=59063.5. A final 4.8-ks observation was obtained on 19 December 2020. The source was not detected in X-rays. The 3-σ count-rate limit is 0.002 ct/s. Using the same model as for the early-time observations, the luminosity is $< 2.3 \times 10^{39}$ erg s^{-1} between 0.3 and 10 keV.

Spectroscopy and Classification

We initiated rapid spectroscopic follow-up of the transient after the initial detection with the SED Machine spectograph (SEDM) (Blagorodnova et al., 2018) on the Palomar 60 inch telescope (on UT 2020-07-31), the Gemini Multi-object Spectro-graph on the North Gemini telescope (Sivanandam et al., 2018) (on UT 2020-07-31) and the Double Beam Spectrograph (DBSP, Oke and Gunn 1982) on the Palomar 200-inch telescope (on UT 2020-08-12). We show the spectral evolution in Figure 2.3. The presence of Balmer lines (Hα and Hβ labeled in Figure 2.3) points towards

the classification of a Type II supernova (Filippenko, 1997; Gal-Yam, 2017). Our spectra also show evidence for P-Cygni profiles from He I and Ca II. The relatively flat light curve is characteristic of the plateau of constant brightness found in those of Type II-P supernova, typically expected to last around 100 days (Branch and J. Craig Wheeler, 2017). Taken together, we classify PGIR20eid as a Type II-P supernova. Using the minimum of the strong P-Cygni profile of the Hα line, we see that the expansion velocities decrease over time. We measured an expansion velocity of 9400 km/s through SEDM, 8800 km/s in the Gemini spectrum, and 7900 km/s in the P200 spectrum, the same order in time that the three spectrographs were triggered.

We also obtain four additional optical spectra, from SEDM again (on UT 2020-08-28), from the Low Resolution Imaging Spectograph on the Keck-I telescope (LRIS,Oke, Cohen, et al. 1995 on UT 2020-11-20), and three more from DBSP (on UT 2021-01-08, 2021-02-20, and 2021-04-16). The latter four spectra show the transition of the SNe into the radioactive decay nebular phase, with characteristic nebular spectra features like the [O I] doublet ($\lambda\lambda$ 6300, 6364) evolving with time with greater line luminosities the further the SN gets into the nebular phase (more in § 2.4).

4 spectra in the NIR were also obtained. These were obtained by the Near- Infrared Echellette Spectrometer (NIRES, Martin et al. 2018 on UT 2020-10-31), and the Triple Spectrograph on the Palomar 200 inch Telescope (TSPEC, Herter et al. 2008), on UT 2020-10-31, UT 2020-12-22, UT 2021-02-04, and UT 2021-05-16. All spectra obtained are shown in Figure 2.3, with characteristic Hydrogen and Helium lines also plotted.

Near-Infrared Spectropolarimetry

The proximity and brightness of SN 2020qmp and the resulting apparent magnitude allowed for spectropolarimetry observations in the IR. Spectropolarimetric observations can constrain the geometry of the ionized, electron scattering region in the SN. IR spectropolarimetry has an added benefit of less contamination from dust polarization along the line of sight, both in the host galaxy and in the Milky Way (Nagao, Maeda, and Tanaka, 2018). We observed the SN on UT 2020-10-29, 91 d post-discovery, while the SN was still in the plateau phase, with the apparent magnitude of $J = 13.2$ mags. The observation was obtained using the IR spectropolarimeter WIRC+Pol on the 200-inch telescope at Palomar Observatory (Tinyanont, M. A.
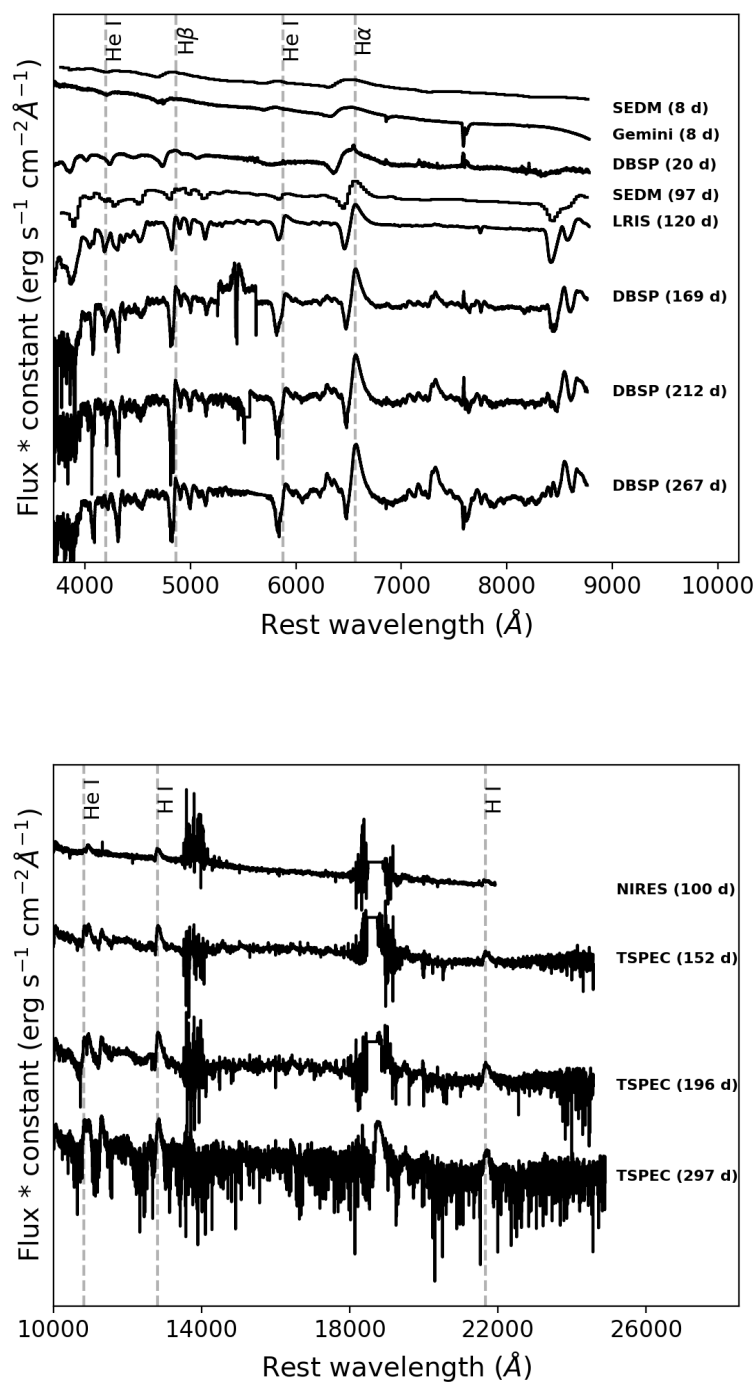
Figure 2.3: *Top panel*: The optical spectra of SN 2020qmp, evolving with time from the top of the plot to the bottom. The epoch and instrument the spectra was taken with are shown to the right of each spectrum. *Bottom panel*: The NIR spectra of SN2020qmp, again evolving with time from the top of the plot to the bottom. The epoch and instrument the spectra was taken with are shown to the right of each spectrum.
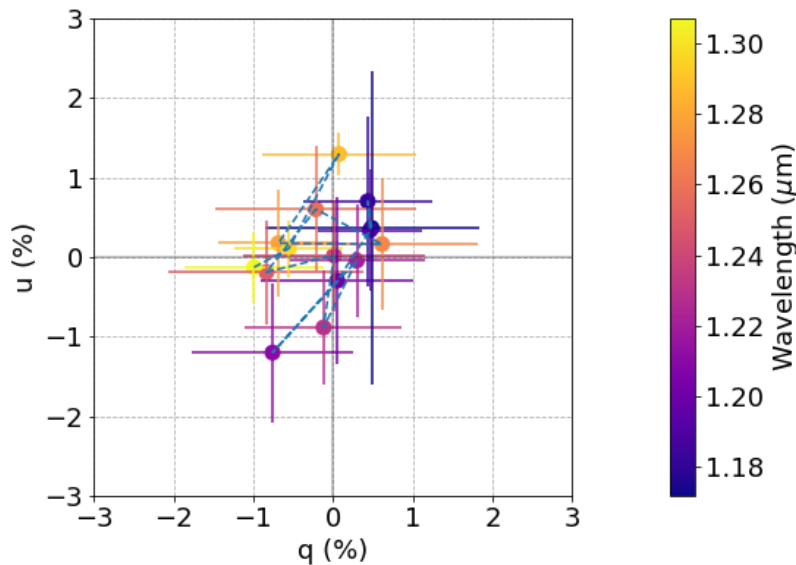
Figure 2.4: J-Band spectropolarimetry on SN 2020qmp conducted by WIRC+POL, on UT 2020-08-29. The panel shows the q-u plane, color coded by wavelength.

Millar-Blanchaer, et al., 2019b; Tinyanont, M. Millar-Blanchaer, et al., 2019). The SN was observed inside its 3″ slit in an ABAB dithering pattern for the total of 64 min of exposure time. The observations were performed at high airmass, resulting in low flux due to the large atmospheric extinction. WIRC+Pol exhibits <0.03% of instrumental polarization, and observations of unpolarized standard stars were not necessary (Tinyanont, M. Millar-Blanchaer, et al., 2019). The data were reduced using the WIRC+Pol data reduction pipeline.[4]

Fig. 2.4 shows the normalized Stokes parameters q and u plotted against each other, color-coded by wavelength. On this plot, the distance from origin is the degree of polarization p while the angle with respect to the x axis is twice the angle of polarization θ. We did not detect polarization from SN 2020qmp, as the broadband degree of polarization was $0.14 \pm 0.26\%$, making tthe SN unpolarized to within 0.78% at the 3σ level. The typical error bar per spectral channel is 1% in both q and u, and the broadband upper limits are 0.25% and 0.27% in q and u, respectively (all 1-σ). The non-detection of polarization of a SN II-P during the plateau phase is consistent with most Type II-P SNe because the outer ejecta, visible during this phase, are generally symmetric (see a review by Wang and J. C. Wheeler, 2008).

---

[4]https://github.com/WIRC-Pol/wirc_drp
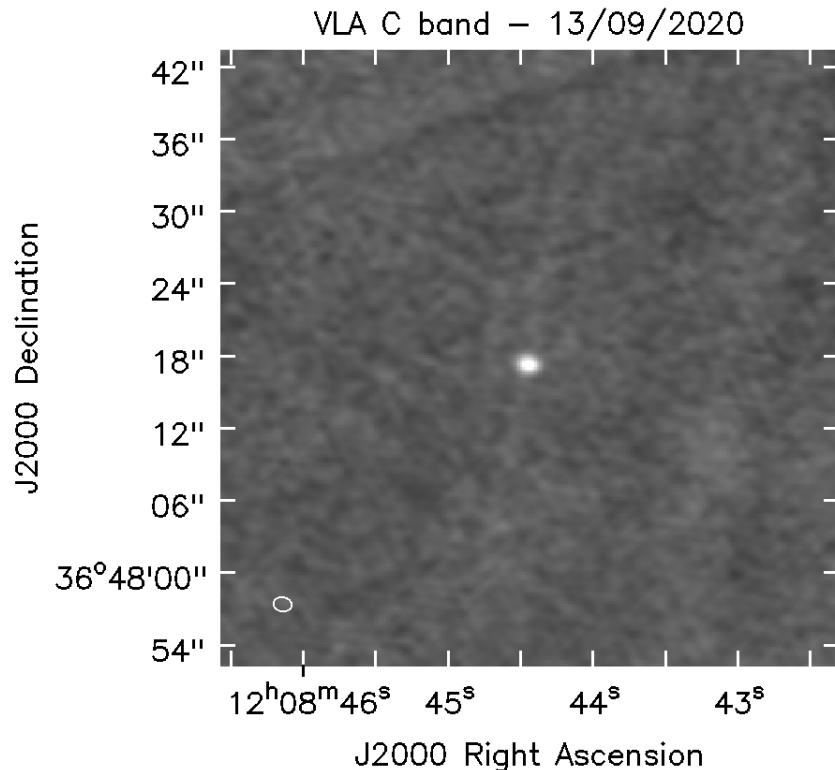
Figure 2.5: Image of the detection of SN 2020qmp in C band by the VLA on UT 2020-09-13.

Observations by VLA

The Jansky Very Large Array (VLA) observed (under our DDT program VLA/20B-398; PI Horesh) the field of SN 2020qmp and detected radio emission consistent with the SN position on four epochs. The first observation, on UT 2020-09-13, showed a point source in both C band (6 GHz) and K band (22 GHz). at a flux level of 0.25 and 0.08 mJy respectively. The detection image in C band is shown in Figure 2.3. We continue monitoring the SN with the VLA using S, C, X, and Ku bands (3, 6, 10, and 15 GHz).

We calibrated our observations with the automated VLA calibration pipeline available in the Common Astronomy Software Applications (CASA) package (McMullin et al. 2007). 3C286 was used as the primary flux calibrator, while J1146+3958 was used as the gain calibrator. When imaging the field of SN2020qmp with the CASA task CLEAN, we divided C and S bands into two sub-bands when the signal-to-noise ratio was high enough. However, due to the relatively low signal to noise ratio, we did not divide higher bands. We used the CASA task IMFIT to fit the source in the phase center and to extract the peak flux density. We estimate its error to be a square

root of the quadratic sum of the error produced by the CASA task IMFIT, the image rms produced by the CASA task IMSTAT, and 10% calibration error. We report the flux measurement in the Appendix.

2.3 Hydrodynamical LC Modeling

It is possible to constrain the ZAMS progenitor mass and initial explosion energy of the SN through hydrodynamical LC modeling (Utrobin and Chugai, 2015; Utrobin and Chugai, 2017; Morozova, Piro, and Valenti, 2017; Morozova, Piro, and Valenti, 2018; Goldberg, Bildsten, and Paxton, 2019; Martinez and Bersten, 2019). In order to do so, we use the open-source SN Explosion Code (SNEC; Morozova, Piro, Renzo, et al., 2015). SNEC assumes local thermodynamic equilibrium (LTE) and diffusive radiative transport, and these assumptions allow it to model LCs well up to the radioactive decay phase, where these assumptions break down. Therefore, we only compare the model LCs generated through SNEC to the observed LCs up to 125 days after the explosion, when the plateau phase has noticeably transitioned to the optically thin nebular phase.

In our analysis, we follow a similar approach to Morozova, Piro, and Valenti (2017), and began by generating optical LCs corresponding to a range of ZAMS progenitor masses between 10.0 $M_\odot$ and 30.0 $M_\odot$ ($\Delta M_\odot = 2.5$), and a range of explosion energies between 0.2 and 1.2×10^{51} ergs ($\Delta E = 0.2 \times 10^{51}$) with models obtained from Sukhbold et al. (2016). We fix the ^{56}Ni mass of the models to $M_{\mathrm{Ni}} = 0.059 M_\odot$, which we obtained using photometry after the radioactive decay tail (see §2.4). It is possible to vary the M_{Ni} in SNEC; however, as mentioned earlier, SNEC does not do well at reproducing LCs after the plateau-phase, and the end of the plateau and beginning of the post-plateau phase is where variations in the ^{56}Ni mass play a significant role in the LC. We then run through a coarse grid of models and perform a χ^2 analysis between the models and observed LCs in the r, g, and i-bands. This χ^2 analysis is done through comparing every observed photometry point from the ZTF LC to the model point closest in time to the observed point, corresponding to the same band filter. The models generate photometry points in units of absolute AB magnitudes, so we convert the model points to apparent AB magnitudes to display in Figure 2.6, but perform the χ^2 analysis in flux space after converting the apparent AB magnitudes to fluxes. We found that the best fitting models are between 10 and 12.75 $M_\odot$ (refer to Figure 2.6). We then ran the SNEC code within a finer parameter space, between 10 and 12.75 $M_\odot$ ($\Delta M_\odot = 0.1$), and again between 0.2 and 1.2 e51 ergs ($\Delta E = 0.1$), and repeat the χ^2 analysis in the finer region to obtain the final
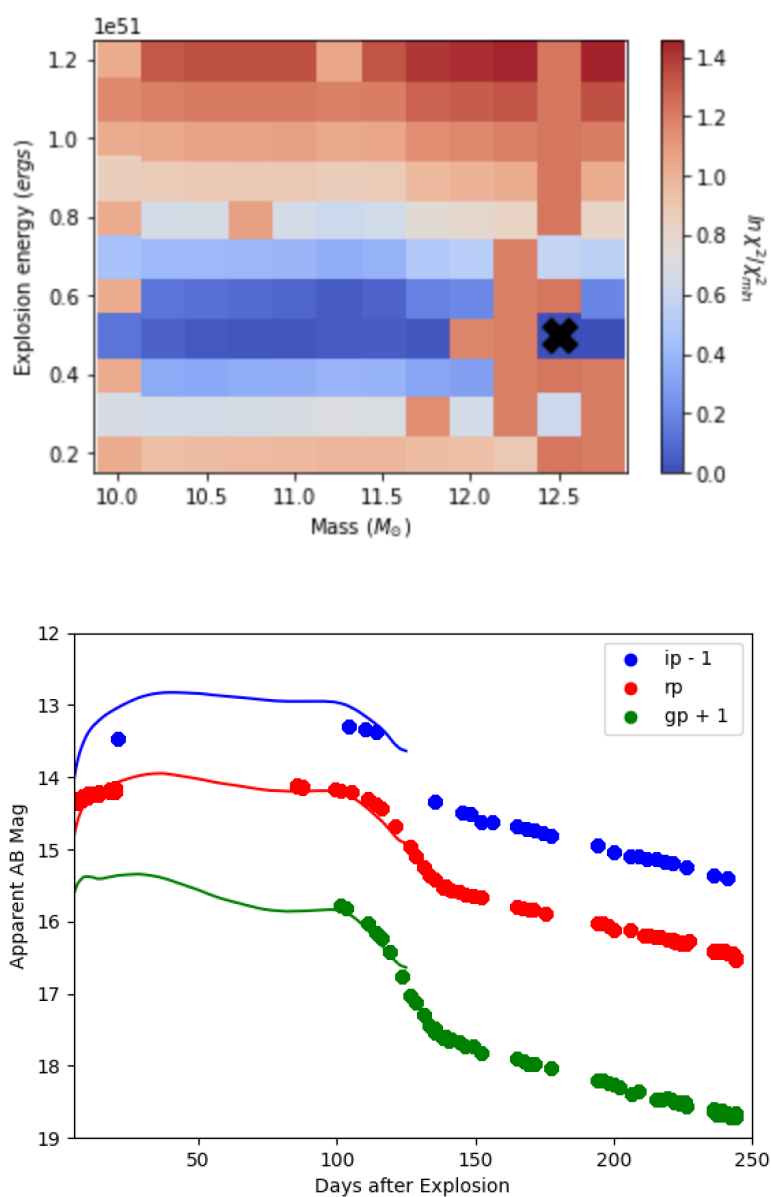
Figure 2.6: *Top panel:* The χ^2 values for the different LC models compared to observations, over a range of 10 to 12.75 $M_\odot$ and an explosion energy of 0.2 to 1.2 $\times 10^{51}$ ergs, with an "X" demarcating the best-fit model. *Bottom panel:* The best-fit LC models in i, r, and g bands , representing a progenitor source of 12.5 $M_\odot$ and an initial explosion energy of 0.5×10^{51}ergs. The models were fit to the observed LC up to 125 days after the explosion.

best-fitting progenitor mass as well as explosion energy. The results of the analysis are shown in 2.3, and we obtain a best-fit ZAMS progenitor mass of 12.5 $M_\odot$, and an initial explosion energy of 0.5×10^{51} ergs, with a $\chi^2_{min} = 1.6 \times 10^{-25}$. This best-fit mass matches well with the ZAMS progenitor mass obtained using an independent method in §2.4 using the nebular spectra. However, it is important to note that this is only a crude estimate of the ZAMS progenitor mass as the LC modeling was able to well constrain the explosion energy, but not the masses as well (as seen in Figure 2.6). Therefore, it was necessary to combine results from the LC modeling and nebular spectrum analysis to find a true estimate of the ZAMS mass.

We note that it is also possible to investigate the effects of the circumstellar medium (CSM) on the early LC, through varying the constant wind density K, extending up to a radius R_{ext} (eg. Dong et al. 2020). K is dependent on both the mass loss rate of the progenitor star, as well as its wind velocity. However, SNEC assumes a standard CSM interaction model with a profile that goes as

$$\rho(r) = \frac{\dot{M}}{4\pi r^2 v_{wind}} = \frac{K}{r^2}, \tag{2.1}$$

which we find might not hold when combining radio and X-ray observations of the SN, as the SN shows possible deviations from a standard CSM interaction model (see §2.5). Therefore, we do not perform further analysis varying K and R_{ext}.

2.4 Nebular Spectrum Analysis

After the photosphere has receded in the ejecta once the hydrogen recombination plateau has ended, the ejecta's inner regions become visible and provide insights into the nucleosynthesis in the explosion occurring. A spectrum taken in this phase after the plateau has declined can also provide key insights into the ZAMS progenitor mass of the source through the comparison of line strengths with existing models, as nucleosynthesis is strongly dependent on the mass of the source. This phase of the LC is called the nebular phase, where the LC becomes dominated by the radioactive decay of ^{56}Ni, In particular, the comparison of the intensities of the [O I] doublet has been shown to provide a good indication of the ZAMS mass (Uomoto, 1986; A. Jerkstrand, S. J. Smartt, et al., 2014), which we use in our analysis.

A. Jerkstrand, S. J. Smartt, et al. (2014) (hereafter J14) developed the models that we use in our analysis. They started with evolved ejecta exploded using KEPLER (Woosley and Heger, 2007), and created the spectra through their former code from Anders Jerkstrand (2011). In Figure 2.7, we show a comparison of these models
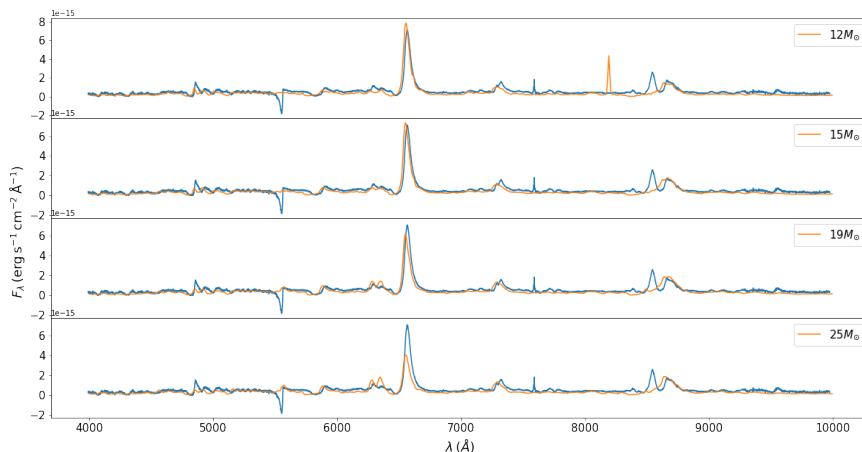
Figure 2.7: Observed (redshift corrected) spectrum of SN 2020qmp in blue at 212 days, overplotted with the models of 12, 15, 19, and 25 $M_\odot$ produced by J14 in orange.

and an observed spectrum taken from the Double Spectrograph (DBSP) on UT 2021-02-20, 212 days after the inferred explosion date. The models are computed at an epoch of 212 days after explosion, for ZAMS masses of 12, 15, 19, and 25 $M_\odot$.

Using these models, along with our observed spectra, we then estimated the ZAMS mass of the progenitor star, by comparing the [O I] doublet line luminosity normalized relative to the ^{56}Co decay power. It is well known that the nebular phase of Type II SNe is driven through the nuclear radioactive decay of ^{56}Ni to ^{56}Co, and then to ^{56}Fe. During this process, γ-rays and positrons are released; however, at this point the ejecta is still not transparent to γ-rays, and as as a result the bolometric luminosity during the nebular phase can be used to determine the ^{56}Ni mass through the relation (Spiro et al. 2014):

$$M_{SN}(Ni) = 0.075 \times L_{SN}/L_{87A}M_\odot \,, \tag{2.2}$$

where L_{SN} is the bolometric luminosity of the SNe in question, and L_{87A} is the bolometric luminosity of SN 1987A. In Figure 2.8, we overlay the bolometric LCs of SN 2020qmp and SN 1987A[5].

After computing the bolometric LCs of SN 2020qmp and SN 1987A, we derived the luminosity 212 days after explosion, and use those values in Eq. 2.2 to estimate $M_{SN}(\text{Ni}) = 0.059\,M_\odot$. After obtaining the ^{56}Ni mass, we then calculated the

---

[5]LC compiled from the Open Supernova Catalog: https://sne.space (Guillochon et al., 2017)
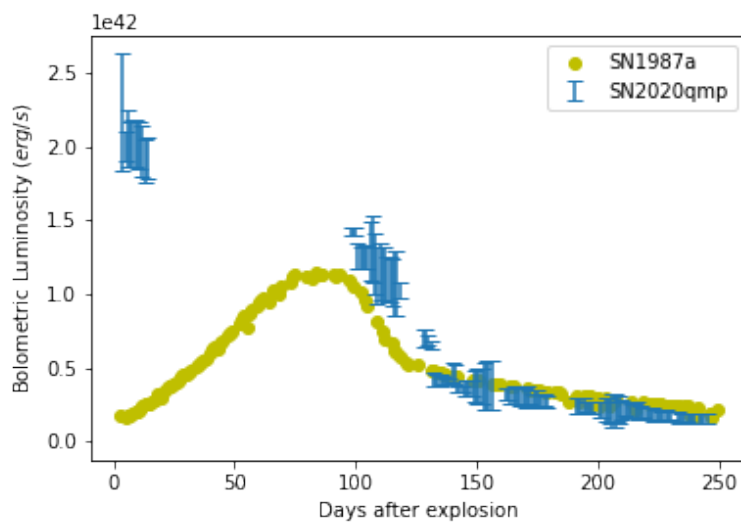
Figure 2.8: Bolometric LCs of SN 2020qmp and SN 1987A.
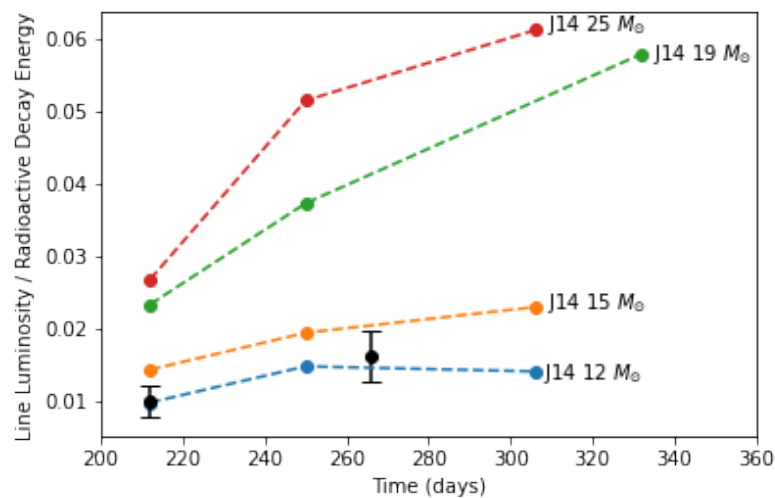
Figure 2.9: The normalized line luminosities of the [O I] doublet ($\lambda\lambda\,6300\,6364$) at different time epochs for the observed spectrum of SN 2020qmp as well as the models from J14.

normalized [O I] doublet line luminosity, relative to the ^{56}Co decay power, which is the main characteristic used to compare model spectra to the observed spectrum. The normalized luminosity is given by J14 as,

$$L_{\text{norm}}(t) = \frac{L_{\text{line}}}{1.06 \times 10^{42} \frac{M_{\text{Ni}}}{0.075 M_\odot} (e^{-t/111.4d} - e^{-t/8.8d}) \text{ erg s}^{-1}}. \quad (2.3)$$

Using the ^{56}Ni mass obtained at 212 days for our observed spectrum, as well as the line luminosity for the [O I] doublet through integrating the line flux subtracted from the continuum by fitting a double-peaked Gaussian function to the spectra, we obtain normalized line luminosities at 212 days and 267 days after the explosion through Eq. 2.3. Then, going through the same process of fitting a double-peaked Gaussian for each of our model spectra, and assuming the same ^{56}Ni mass, we also obtained normalized line luminosities for each model spectra and compare the results in Figure 2.9. We see that the normalized luminosities obtained for the observed spectrum and 12 $M_\odot$ model are equivalent within error bars. This allows us to infer that the progenitor star is close to 12 $M_\odot$. These results agree with the results we found in §2.3, which gave us a progenitor mass of around 12.5 $M_\odot$.

2.5 Modeling the radio data combined with optical and X-ray

The radio spectra is presented in Fig. 2.10. It shows optically thin emission (at $\geq$ 5 GHz) 51 days after the explosion, while the 57 day spectrum shows a turnover into an optically thick spectrum at lower GHz frequencies, at around 4 GHz. However, the turnover frequency is not well constrained due to scarce data at the optically thick regime. On day 104, an optically thin spectrum is observed down to a frequency of 2.31 GHz, surprisingly at a significantly higher flux level at frequencies lower than the turnover frequency observed earlier. The last spectrum, 136 days after the explosion, exhibits optically thin emission with a possible turnover at the lowest observed frequency at around 2.3 GHz. This turnover frequency is even less constrained than the one at 57 days after the explosion. Next, we discuss the radio data in light of a SN-CSM interaction model, and derive the shock physical parameters, e.g. radius and magnetic field strength and the inferred shock velocity and progenitor's mass-loss rate. We finish by using the X-ray and optical data combined with the radio to estimate the shock micro-physical parameters and discuss their effect on our shock properties estimates.
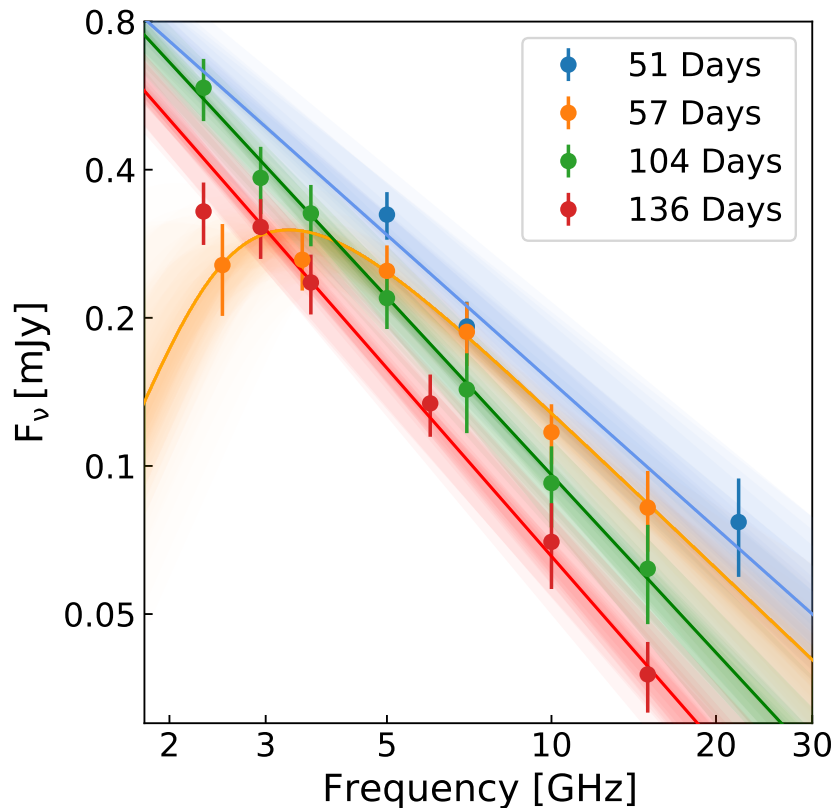
Figure 2.10: VLA spectra of SN 2020qmp at four different epochs. The lines are fitted models as discussed in §2.5, with a shaded confidence region of 1σ. A synchrotron emission model as presented in Eq. 1 in Roger A. Chevalier, 1998, was fitted to the spectrum 57 days after the explosion. An optically thin power law model was fitted to the spectra 51, 104, and 136 days after the explosion.

Modeling the Radio Spectra

When the SN ejecta interacts with the CSM, it drives a shock-wave into it. At the shock front, electrons are accelerated to relativistic velocities with a power-law energy density distribution, $N(E) \propto E^{-p}$, where p is the electron spectral index. The magnetic field is also enhanced at the shock front. The relativistic electrons that gyrate in the presence of that magnetic fields give rise to synchrotron emission which is usually observed in radio frequencies (R. A. Chevalier, 1982). The intrinsic synchrotron emission might be absorbed by synchrotron self-absorption (SSA; Roger A. Chevalier 1998) and/or free-free absorption (FFA; Wieler et al. 2002). The optically thin regime of the spectrum is expected to be a power law of $\nu^{-\beta}$, when in the absence of cooling (e.g. inverse Compton cooling), we expect a constant power-law $\beta = (p - 1)/2$. The full shape of the spectrum as a function of

the radio emitting shell radius and the magnetic field strength is shown in Eq. 1 in Roger A. Chevalier, 1998.

We first modelled the optically thin spectra on 51, 104, and 136 days after the explosion as power-law functions of the form, $F_\nu \sim \nu^{-\beta}$. We do not use the data at the lowest frequency on day 136 as it might feature a turnover (and thus a deviation from a simple power-law function). We performed a χ^2 minimization fit. For the first spectrum (51 days), the fit resulted in $\beta = 0.99 \pm 0.06$ with a minimum $\chi^2 = 1.58$ for one degree of freedom (dof). However, this is based only on three data points and therefore should be treated carefully. For the spectrum on day 104, we find $\beta = 1.20 \pm 0.06$ with a minimum χ^2 of 0.5 (for five dof). The fit of the last epoch (136 days) resulted in a power law of $\beta = 1.27 \pm 0.06$ with a minimum χ^2 of 0.34 (for three dof). The above fits, with their 1σ confidence interval, are shown Fig. 2.10. These power-laws correspond, in the non-cooling regime, to $p = 2.98 \pm 0.12$, 3.40 ± 0.12, and 3.54 ± 0.12, for the first, third, and forth spectrum, respectively. However, the actual value of p will differ if cooling effects are taking place, i.e., if its real value is $p = 3$ then the rather steep spectral slopes may suggest that there is cooling in effect. We also note that we see a change, larger than 2σ, in the electrons power law between the first spectrum and the later ones. Even so, the first spectrum is based only on three points, and therefore the electron power-law inferred from it is questionable.

We next modeled the radio spectrum we observed 57 days after the explosion, a spectrum which exhibits a spectral turnover. To derive the shock physical parameters we fit Eq. 1 in Roger A. Chevalier, 1998. The free parameters are the radio emitting shell radius, R, the magnetic field strength, B, and the power-law of the electron energy density, p. We assume an emission filling factor of 0.5, and equipartition between the the fraction of energy deposited by the shock to the relativistic electrons (ϵ_e), and the magnetic fields (ϵ_B). We use `emcee` (Foreman-Mackey et al. 2013) to preform an MCMC analysis to determine the posteriors of the parameters of the fitted model (and use flat priors). Based on the results of our fit we find that the radius of the emitting shell is $\left(5.46^{+0.96}_{-0.7}\right) \times 10^{15}$ cm, the magnetic field strength is $0.46^{+0.19}_{-0.15}$ G, and $p = 3.12^{+0.43}_{-0.39}$. Assuming a constant shock velocity, i.e., $v_{sh} = R/t$, where t is the time since explosion, we derive $v_{sh} = \left(1.11^{+0.19}_{-0.14}\right) \times 10^4$ km/s.

The CSM, shocked by the SN ejecta, is a result of mass-loss from the progenitor star prior to explosion. Using the results of radio emission modeling above, we can estimate a mass-loss rate, assuming a constant mass-loss rate via a constant
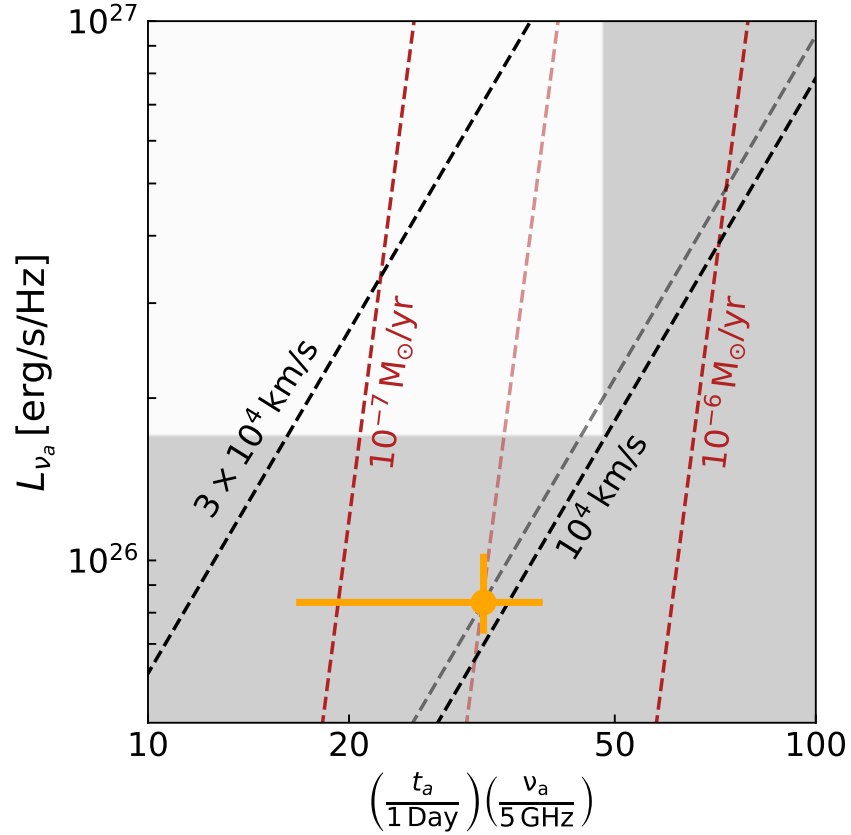
Figure 2.11: Chevalier's diagram for SN2020 qmp. The shaded region is the ruled out region derived from the limit on the peak flux 104 days after the explosion. The orange point is the position of the peak derived 57 days after the explosion. Equal lines of shock velocities and mass-loss rates (assuming a wind velocity of 10 km/s) are also plotted.

velocity stellar winds. Under this assumption, the CSM density structure has a form of $\rho \sim \frac{M}{v_w} r^{-2}$, where M is the mass-loss rate and v_w is the wind velocity. Assuming that the magnetic field energy density is a fraction ϵ_B of the post-shock energy density $\sim \rho v_{sh}^2$, and a constant shock velocity, the mass-loss rate is given by

$$M = 5.2 \times 10^{-8} \left(\frac{\epsilon_B}{0.1}\right)^{-1} \left(\frac{B}{G}\right)^2 \left(\frac{t}{10\,\text{Days}}\right)^2$$

$$\times \left(\frac{v_w}{10\,\text{km/s}}\right) M_\odot/\text{yr}. \quad (2.4)$$

Thus, assuming $\epsilon_B = 0.1$, the mass-loss rate derived from the fitted model for the 57 days after explosion is $M = \left(3.57^{+3.57}_{-3.41}\right) \times 10^{-7} M_\odot/\text{yr}$, for an assumed wind velocity of 10 km/s. The CSM interaction model with the assumptions presented above predicts a constant peak flux that is traveling to lower frequencies with time, for an

assumed CSM structure of r^{-2}. However, the peak flux 104 days after the explosion, despite not being observed, is higher than the observed peak flux on 57 days after the explosion. A useful tool to examine this discrepancy between the two peaks is the phase space of peak spectral luminosity vs. the time of the peak times its frequency. Lines of equal shock velocity, and equal mass-loss rate can be plotted in this phase space, also known as Chevalier's diagram. Fig. 2.11 is showing Chevalier's diagram for SN2020qmp, with the peak inferred from the spectrum 57 days after explosion, which was obtained by fitting the spectrum with Eq. 4 in Roger A. Chevalier, 1998. Also shown in this figure is a shaded region that marks the ruled out regions given the limit on the peak flux and frequency 104 days after explosion. Lines of equal shock velocities, and of equal mass-loss rate for typical values, and for the values derived by the peak at 57 days, are also plotted. We assumed here wind velocity of 10 km/s and $p = 3$. As seen in the figure, the peak flux changes significantly (more than 3σ) between the two epochs. This suggests that (when assuming a constant shock velocity) we observe a significant variation in the mass-loss rate, by about a factor of two. Furthermore, the lowest observed frequency on day 136 might feature a spectral turnover. If indeed that is the case, this point towards additional variability in the CSM structure. However, we emphasize that since this is based only on one point it should be treated with caution.

Possible Deviation from equipartition

The results of our radio emission modeling above are sensitive to the assumption of the ratio between the fraction of shock energy that goes into electron acceleration (ϵ_e), and the fraction of energy that goes into the enhanced magnetic field (ϵ_B). In our analysis above we have used the common assumption of equipartition ($\alpha \equiv \epsilon_e/\epsilon_B = 1$). However, deviations from equipartition have been observed before in several SNe (e.g. SN2011dh Soderberg et al. 2012; Horesh, Stockdale, et al. 2013b, SN2012aw; Yadav et al. 2014, SN 2020oi; Horesh, Sfaradi, et al. 2020). Typically, when one has only radio data, it is difficult to determine whether this assumption holds. However, given X-ray observations, we can try and estimate these micro-physical parameters. We extrapolate the radio spectrum we have 57 days after explosion to the time of X-ray observations according to a typical power law for the optically thin regime of $F_\nu (t) \sim t^{-1}$ (Roger A. Chevalier, 1998). This gives an estimated luminosity of 2×10^{36} erg/s at the Swift/XRT band. This is three orders of magnitude lower than the observed X-ray luminosity at that time. Thus, even if the extrapolation of the radio emission to early times and the X-ray band is

somewhat crude, there is evidence for significant excess in X-ray emission.

Björnsson and Claes Fransson, 2004 suggested inverse Compton (IC) scattering of photospheric photons by relativistic electrons at the shock front as a possible emission mechanism in the X-ray. IC scattering is also assumed to be responsible for the observed X-ray emission in several past SNe (e.g. SN2011dh; Horesh et al. 2014, SN2012aw; Yadav et al. 2014, SN2020oi; Horesh, Sfaradi, et al. 2020). We use Eq. 32 in Roger A. Chevalier and Claes Fransson, 2006 to estimate the mass-loss rate given the X-ray luminosity of 2×10^{39} erg/s, 8.8 days after explosion, and the bolometric luminosity of 2.14×10^{42} erg/s at that time. We assume a shock velocity of 10^4 km/s based on the optical photospheric expansion velocity of $\sim$ 9000 km/s from optical emission near that time. This velocity is expected to be somewhat slower than the velocity of the shock in the CSM since it originates from a deeper and slower region of the SN ejecta.

The derivation of the mass-loss rate, using the X-ray emission, requires an assumption on the micro-physical parameter ϵ_e. Assuming a typical $\epsilon_e = 0.1$ we infer a mass-loss rate of $9.31 \times 10^{-6} \, M_\odot$/yr for an assumed wind velocity of 10 km/s. The mass-loss rate derived from the radio spectrum 57 days after the explosion is smaller by a factor of 26. A possible explanation for this discrepancy is that the mass-loss rate is constant over time, but there is deviation from equipartition, such that satisfy $\epsilon_B = 3.6 \times 10^{-4}$, which in turn translates to $\alpha = 280$ (assuming a typical $\epsilon_e = 0.1$). This also results in reduction of the shockwave radius, and the resulting shock velocity, derived from the radio spectrum on day 57 by 26%, which means $v_{sh} = 8250$ km/s. We can also explain this discrepancy with a decrease in mass-loss rate from the progenitor in the years prior to the explosion, by a factor of 26. Moreover, mass-loss variation is also indicated by the difference in the radio peak flux between day 57 and 104, which implies an increase in mass-loss rate by a factor $\sim$ 2. However, this is still in strong disagreement with the value of mass-loss rate inferred by the X-ray emission. If indeed mass-loss variations responsible for these discrepancies, the progenitor of SN2020qmp experienced a unique mass-loss history in the years before the explosion.

2.6   Local CCSNe rate and Infrared Surveys

Most massive-star formation, and therefore their resulting CCSNe at the end of their lives, occurs in highly extincted regions in the universe where observations are obscured highly by dust. Therefore, uncovering the rate of nearby CCSNe is highly

dependent on the effects of dust and extinction (Grossan et al., 1999; Maiolino et al., 2002) As a NIR survey, PGIR is sensitive to CCSNe that may be obscured at optical wavelengths due to high extinction values. Though SN 2020qmp itself is not highly extincted at optical wavelengths (line-of-sight $A_V \approx 0.069$ according to Schlafly and Finkbeiner (2011)), its detection invites the question as to how effective NIR surveys are in detecting obscured SNe in comparison to optical surveys.

Mattila et al. (2012) derived a CCSNe rate of $7.4^{+3.7}_{-2.6} \times 10^{-4} \mathrm{yr}^{-1} \mathrm{Mpc}^{-3}$ within the local 6 Mpc volume and $1.5^{+0.4}_{-0.3} \times 10^{-4} \mathrm{yr}^{-1} \mathrm{Mpc}^{-3}$ within the local 6-15 Mpc volume, using a 12 year sample of CCSNe from 2000-2012. However, they also derived an estimate of $18.9^{+19.2}_{-9.5}\%$ of CCSNe missed locally by optical surveys. Furthermore, this number has been estimated to be as high as $38.5^{+26.0}_{-21.9}\%$ by Jencson et al. (2019), based on extremely extincted SNe detected from the Spitzer Infrared Intensive Transient Survey (SPIRITS) mid-infrared survey (Mansi M. Kasliwal et al., 2017). Here, we provide an estimate of PGIR and WINTER's (a future NIR survey in J-band) sensitivity to detect CCSNe within the local universe.

Richardson et al. (2014) calculated the bias-corrected absolute magnitude distributions of SNe primarily from the Asiago Supernova Catalog (Tomasella et al., 2014) as well as a few supplemental data sources. Through averaging their distributions for all types of CCSNe, and weighing them appropriately with the number of events, we obtain an estimate of the average magnitude for any CCSNe to be $M_{abs} = -17.42 \pm 0.37$ in B-band. Assuming this absolute magnitude, in Figure 2.12 we show the sensitivity of PGIR in detecting CCSNe with respect to their distance and extinction values in J-band. Performing synthetic photometry assuming a blackbody spectrum of 10,000 K, we compare the sensitivity curves to the ZTF g and r-bands. Figure 2.12 shows that PGIR is more effective in detecting obscured CCSNe in the very local universe, which is telling because its median depth is ∼ 5 mag shallower than ZTF, which has a median depth of around 20.5 AB mags (Masci et al., 2018). Specifically, using our formulation detailed above, PGIR is more sensitive to extincted CCSNe until ∼ 6.4 Mpc in ZTF's r-band and 12.7 Mpc in ZTF's g-band. We also add a sensitivity curve for WINTER, which will be able to see up to a median depth of 20.9 AB mag in J-band (Simcoe et al., 2019; Lourie et al., 2020; Frostig et al., 2020). WINTER is based out of Palomar observatory expected to have first light in Fall 2021.

Using the sensitivity curves, in Figure 2.13 we show the results of a simulation representing a distribution of CCSNe with varying extinctions and distances. In
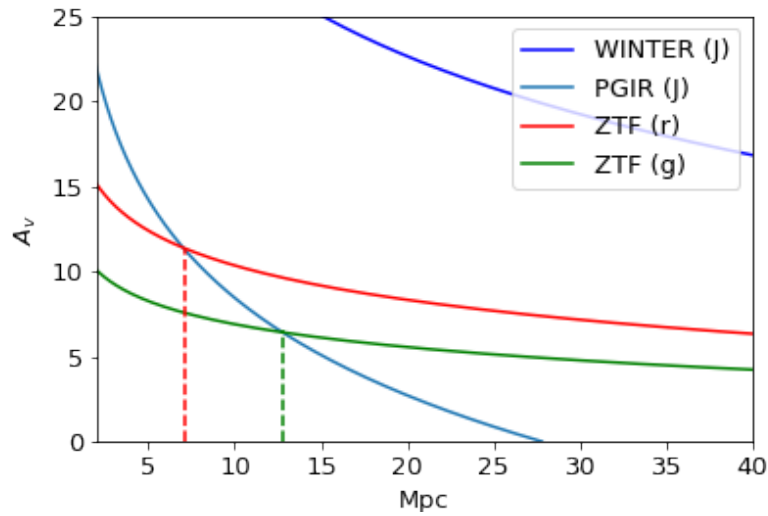
Figure 2.12: Comparison of PGIR's sensitivity to detecting CCSNe as a function of distance and extinction to that of ZTF's *r* and *g* bands. WINTER's sensitivity curve is also overlain in the plot.
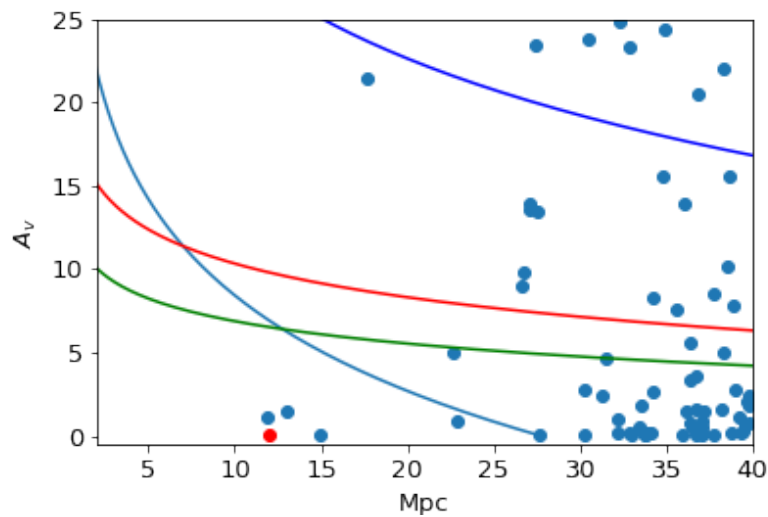
Figure 2.13: Simulated supernovae over a five year span using the extinction distribution of (Jencson et al., 2019). Details of simulation in text, with the same sensitivity curves as Figure 2.12. SN 2020qmp in particular is marked in red to demonstrate its placing in the simulated distribution.

order to model the extinction distribution, we pull from the CCSNe sample detailed in Jencson et al. (2019), using their sample of optical and infrared discovered transients by SPIRITS. We assume the upper limit A_V values for those with upper limits, and extinction values of $A_v = 8$ mag for those with lower limits, which is around the highest value of the observed A_V in the infrared sample. We fit a power law to these values, sorted by ranks, to determine their cumulative distribution function, and from there derive a probability distribution function for A_V values of CCSNe. Next, using the CCSNe rates (Mattila et al., 2012) as well as taking into account the field of view of PGIR, we derive a similar probability distribution function for distance values of CCSNe. Finally, we run the simulation created from the probability distribution for 75 hypothetical CCSNe, assuming a 5 year sample, and run the simulation 10 times. A single run of our simulation is shown in Figure 2.13, and over the 10 simulations, we find that PGIR is likely to not detect any CCSNe that ZTF will miss due to dust extinction effects in a five year time period. This is mainly due to the fact that PGIR's median depth is much lower than that of ZTF's. However, when looking at future NIR surveys such as WINTER, we find a much higher number of projected CCSNe to be discovered- around 14 averaged over our 10 simulations. WINTER's median depth is around the same of ZTF's, demonstrating the impact that NIR surveys can have on discovering CCSNe in the future.

2.7 Conclusion

In this paper, we presented a detailed, multi-wavelength analysis of SN 2020qmp discovered by PGIR. Based on characteristic Hydrogen lines in its spectra, along with a long plateau in its optical LC, the SN can be classified as a Type II-P SN. We do not detect any polarization from the SN during the plateau phase, which is consistent because the outer ejecta are generally symmetric (Wang and J. C. Wheeler, 2008). Through hydrodynamical LC modeling using SNEC, we obtain a best-fit progenitor mass of around $12.5 M_\odot$ and explosion energy of 0.5×10^{51} ergs, though only the explosion energy was well-constrained. By comparing the normalized line luminosities of the [O I] doublet (relative to the ^{56}Co decay energy) between the observed spectrum and J14 models, we estimate the progenitor mass of the SN to be $\approx 12 \, M_\odot$, consistent with the results found through the hydrodynamical LC modeling.

We also made use of broadband radio observations conducted with the VLA to derive the physical properties of the shock in the CSM under the CSM interaction

model. Assuming equipartition between the fraction of energy in the electron (ϵ_e), and the fraction of energy in the enhanced magnetic field (ϵ_B), the radio spectrum 57 days after the explosion gives a shock velocity $v_{sh} = 1.11 \times 10^4$ km/s, and a mass loss rate of M $= 3.57 \times 10^{-7} M_\odot$/yr, for an assumed wind velocity of 10 km/s. However, the radio spectrum on day 104 showed a surprisingly higher peak flux at lower frequency than the one observed on day 57. We determine that assuming standard CSM interaction models, and constant shock velocity, an increase in mass-loss rate by a factor of ~ 2 is needed to explain this discrepancy. This and additional radio observations on day 136 points to variability in the progenitor mass-loss rate during the 1000 years prior to explosion.

Early X-ray observations with Swift/XRT show excess emission compared to the one extrapolated from radio frequencies to early times using standard shockwave evolution. Assuming that this emission excess originates from inverse Compton scattering of photospehric photons by relativistic electrons in the shock front, we derive a much greater mass-loss rate than the one derived by the radio spectrum on day 57, of M $= 9.31 \times 10^{-6} M_\odot/yr$, for an assumed wind velocity of 10 km/s. This discrepancy can be resolved assuming deviation from equipartition of $\epsilon_B = 0.00036$ and $\epsilon_e = 0.1$. This also calls for a reduction in the inferred shock velocity by 26%, from 1.11×10^4 km/s to 8.25×10^3 km/s. One can also explain the difference in mass-loss rates by extreme mass-loss variations from the progenitor in the years prior to the explosion.

Finally, we created a simulation of CCSNe within a five year span. We assumed CCSNe rates from Mattila et al. (2012), and extrapolating an extinction distribution from Jencson et al. (2019), assuming an absolute magnitude of -17.427 for every SN calculated through taking a weighted distribution of the CCSNe sample given in Richardson et al. (2014). Though SN 2020qmp itself is not extremely extincted, its discovery prompted the question as to how much more sensitive PGIR is than optical surveys such as ZTF to extincted SNe as a NIR survey. We find that in a five year span, that we expect PGIR to detect no CCSNe that ZTF misses, and this is due to the much lower median depth that PGIR has in comparison to ZTF. However, this number shoots up when looking at future NIR surveys such as WINTER, with higher median depths comparable to those of ZTF, where we estimate around 14 CCSNe to be discovered that are missed by ZTF. This shows how promising future NIR surveys will be for discovering extincted CCSNe.

C h a p t e r   3

STUDYING CCSNE RSG PROGENITORS

As mentioned in Chapter 2, galactic and extremely nearby extragalactic CCSNe are extremely uncommon, especially with respect to the hundreds of more distant extragalactic CCSNe detected every year. Therefore, when the next nearby CCSNe goes off, it is paramount to be able to rapidly discover the CCSNe right after explosion, so that telescopes ranging over all wavelengths can be pointed at the location of the explosion in order to gather invaluable data across the electromagnetic spectrum. Identifying nearby CCSNe shortly after explosion will also allow for neutrino and gravitational wave detections to be made, providing deeper insights into supernova physics than possible from just the electromagnetic spectrum.

Monitoring nearby RSGs through obtaining their photometric data is an important tool that can be used to prepare for rapid follow-up observations for the next nearby CCSNe, as understanding the variability of RSG LCs near the end of their lives could provide key insights into the early core-collapse process. Nakamura et al. (2016) provides a complete list of nearby RSG candidates, compiled from literature. These 213 candidates are all within 3 kpc, which is the maximum distance for detecting pre-CCSNe neutrinos for the most advanced neutrino detectors, and is also close enough for small telescopes to be able to detect the source. Because many of these candidates are located in the direction or close to the galactic center, they are obscured by large columns of line-of-sight extinction at optical wavelengths.

This is where NIR detectors such as PGIR are invaluable, as they are largely transparent to dust extinction effects due to operating in J-band. This puts PGIR in a unique position, as it has the potential to be able to produce incredibly robust NIR LCs of RSGs. Combining these NIR LCs at the end of the progenitor RSG lives with neutrino and GW observations shortly after the explosion will open up a new window into understanding the processes driving RSGs to explode into CCSNe, which is a very active area of research in supernova physics.

However, these extremely nearby RSGs from Nakamura et al. (2016) are very bright in J-band (a histogram detailing the distribution of magnitudes of each of the RSGs in the sample is shown in Figure 3.1), and PGIR's detector had limitations that did not allow us to image such bright targets. The rest of this chapter will detail the
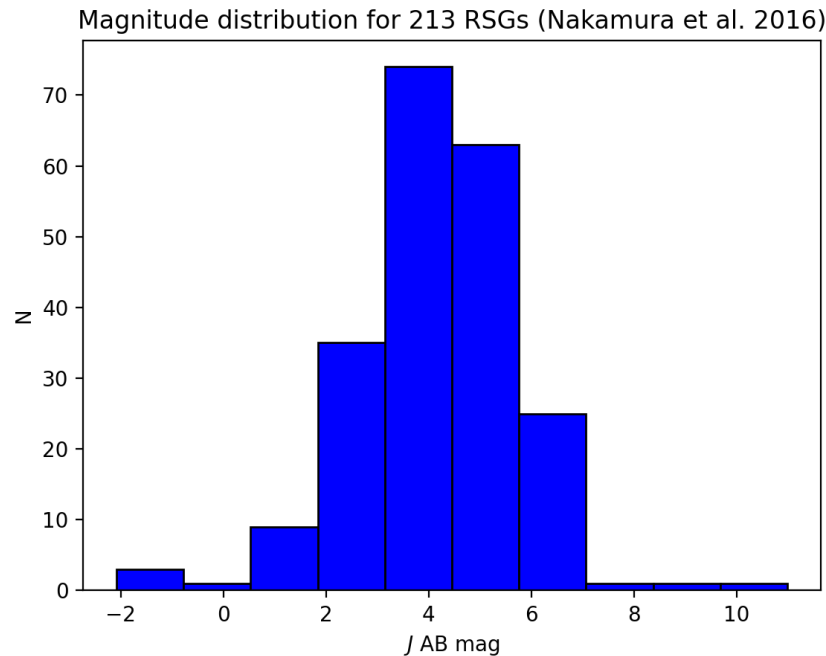
Figure 3.1: Histogram detailing the *J*-magnitude distribution of the list of nearby RSGs compiled by Nakamura et al. (2016)

technical specifications of PGIR, and how we were able to increase the dynamic range of PGIR, giving us the ability to image many of the RSGs from the sample of Nakamura et al. (2016). We will conclude with a short discussion on the implications of this work, and future directions for PGIR.

3.1 Technical specifications of PGIR

PGIR utilizes a state-of-the-art approach with the use of rapid optics in order to obtain a large pixel scale and field of view that allows for PGIR to survey the entire accessible sky every two nights (K. De, Hankins, M. Kasliwal, et al., 2020). PGIR's aperture was set to 0.3 m in order to allow for a sensitivity of around 15.7 AB mag in J band, and uses a f/1.44 refractive optical telescope assembly called Terebizh TEC300VT. The optical design only needed to be slightly modified with a slight focus adjustment as well as a NIR coating on the lens in order to reach the necessary sub-pixel image quality needed all the way across the J band spectrum (K. De, Hankins, M. Kasliwal, et al., 2020).

PGIR's detector is a 2K × 2K Hawaii2RG (H2RG) detector. The detector is made out of mercury cadmium telluride (HgCdTe), initially on a cadmium zinc telluride

(CdZnTe) substrate. The detector comes with three cutoff wavelength options, calculated where it achieves a value of 50% quantum efficiency- 1.75 μm, 2.5 μm, and 5.3 μm. PGIR chose the 1.75 μm option, which was a calculated move in order to avoid the thermal Cosmic Infrared Background that peaks above 2 μm (K. De, Hankins, M. Kasliwal, et al., 2020). The detector also makes use of a technique called substrate-removal, where the CdZnTe substrate layer is removed after the detector is hybridized to the Readout Integrated Circuit of the detector. Removing the substrate results in a large increase in quantum efficiency under 1.3 μm (Jerram and Beletic, 2019)- perfect for PGIR's operations at the 1.25μm level where it obtains a high quantum efficiency of 70%. The pixel size of the detector is 18 μm, and the detector is 2048 x 2048 pixels. Pairing this with the f/1.44 focal beam of the telescope, PGIR achieves a plate scale of 8.73"/pixel, which is significantly larger than any other ground-based NIR detector (K. De, Hankins, M. Kasliwal, et al., 2020). Finally, the gain and read noise of the detector are 4.5 e^-/ADU and 25 e^- respectively. Because the NIR sky background counts is much greater than any dark current count over a range of infrared detectors, the dark current (0.9 e^-/s) is essentially negligible with respect to the signal-to-noise ratio for PGIR.

3.2 Implementation of New Readout Mode

With regards to the readout electronics of PGIR, PGIR originally operated with its old readout mode until May 2020, when a new readout mode replaced it. Initially in the old readout mode, the detector read out each pixel with a readout time of 6 μs, with 2 μs settling time for each pixel after excitement and 4 μs actual integration time (K. De, Hankins, M. Kasliwal, et al., 2020), which leads to a single frame being read out in 0.79 seconds. Originally, PGIR would take 8.1 seconds for each exposure (in a set of 8 dithers per field). However, this readout mode had disadvantages. When an exposure started, the system would wait until the next frame began, and then would reset and read the reset frame. Following that, it would wait 8.1 seconds before reading the end-of-exposure frame, and the science image stored was the difference between that final readout and the reset frame. This readout mode was not very efficient, as up to a frame-time (0.79 seconds) was lost while waiting for the reset frame to be taken, and more frame-times were lost while waiting for all of the data to be written to the disk after the final exposure. Furthermore, due to the long exposure time of 8.1 seconds, the detector saturated at just 8.5 AB magnitudes.

Due to these disadvantages, a new readout mode was then implemented. In this readout mode, the detector is constantly reading out, and the data is stored in a

"ring buffer" that is able to store the last ten frames taken. Because the data is continuously stored as the detector is being read out, there is no time wasted, unlike in the previous readout mode where we had to wait for the exposure to begin or for the data to be stored in the disk. Furthermore, the pixel readout time is also cut by half to 3.1 μs, which gives a frame time of 0.85 seconds for both the reset frame followed by an end-of-exposure frame. Longer exposures are created by adding up these end-of-exposure frames, but the saturation limit is brought down because we have effective exposure times of 0.85 seconds, rather than the 8.1 seconds of the old readout mode. This brings the saturation limit down by 2.5 magnitudes to around 6 AB magnitudes.

However, even in this mode, the saturation limit of 6 AB magnitudes is still not enough to be able to measure the majority of sources in the catalog compiled by Nakamura et al. (2016), as the majority are greater than 6 AB magnitudes in *J*-band. In order to increase the dynamic range even more, we make use of "short exposures" in the new readout mode. In order to do this, instead of just alternating between reset frames and end-of-exposure frames like mentioned earlier, there is an additional short exposure readout added after the end-of-exposure frame, which brings the effective exposure time up to 1.27 seconds from 0.85 seconds. This may seem counter-intuitive, as it decreases the dynamic range increase from 2.5 magnitudes to 2 magnitudes.

However, this 2 magnitude increase in dynamic range can be made larger by choosing to use only the short exposures, where we can choose the amount of row-times to use for each exposure. Nominally speaking, the lower number of row-times we choose, the higher the increase in dynamic range we can achieve. However, when trying to understand the optimal amount of row-times to use for the short exposure, PGIR had to wrestle with non-linearity in the photometry obtained in this new readout mode. This occurred due to intrinsic heating effects originating from the detector, where pixels after a readout would still be excited to values above their baseline continuum even after resetting, leading to to larger photometry values than those truly from the source.

This effect can be seen quantitatively in Figure 3.2, which depicts the counts obtained from aperture photometry of a well known star. We realized that using extremely low row-times led to non-linear effects, and we attempted to fit an exponential rise to linear function to predict these effects. However, the fit was not close to converging to the photometry obtained from the normal, long exposure at 1.27 seconds, which
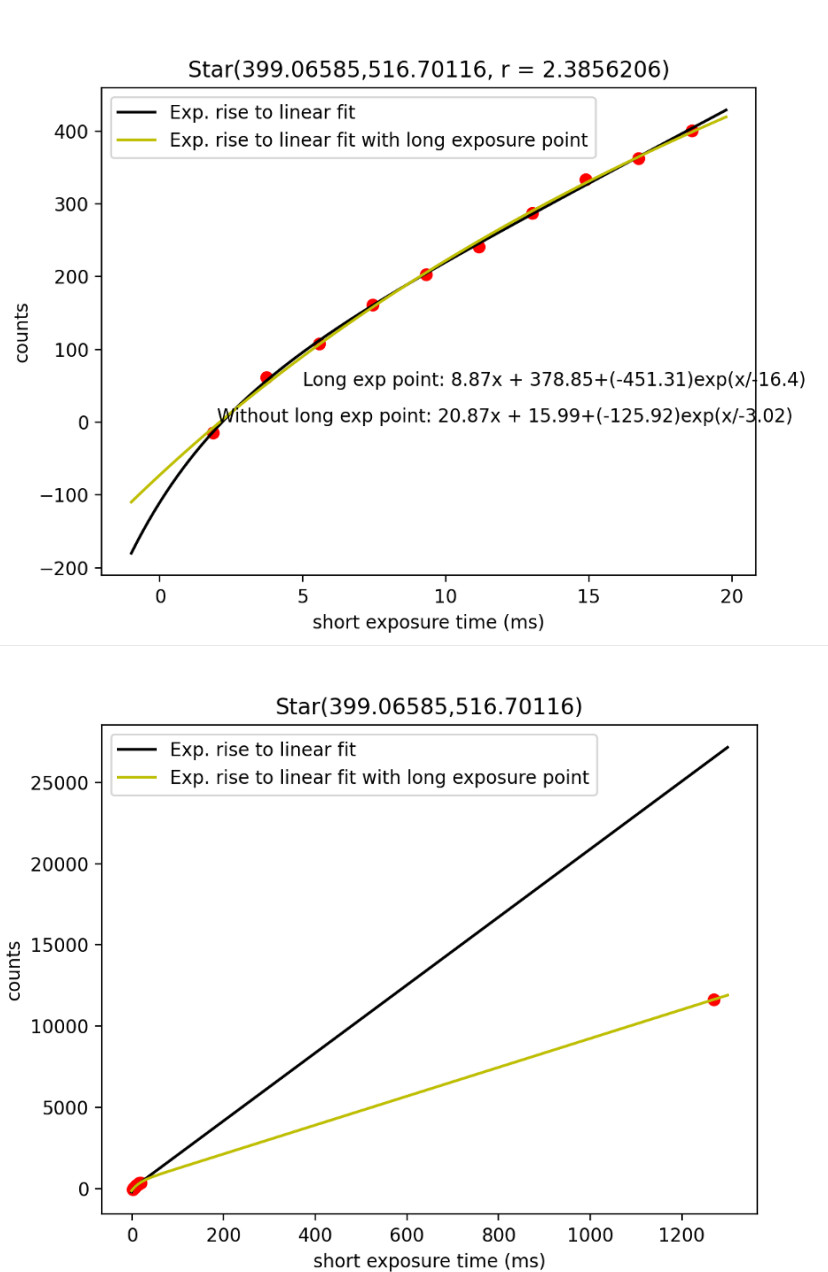
Figure 3.2: *Top panel:* A plot showing exponential rise to linear functions fitted to the aperture photometry count values obtained through different short exposure times. *Bottom panel:* A zoom-out of the plot in the top panel, showing the counts obtained in the long exposure of 1.27 seconds

has the most accurate count rate intrinsic to the source.

In order to strike a middle-ground between being able to image brighter targets without saturating as well as avoiding unpredictable non-linearity, we decided on using 100 row-times, or exposure times of around 0.065 seconds. This exposure time gives an additional improvement in dynamic range of 3.3 magnitudes, in addition to the 2 magnitudes gained from the new readout mode with the short-exposure, while avoiding the heating effects intrinsic to the detector. This is a 5.3 magnitude increase in dynamic range from the old readout mode, which theoretically allows PGIR to image sources as bright as 3.2 AB magnitudes.

3.3 Future Directions

With the implementation of the new readout mode and the use of the short exposures, PGIR now has the potential to obtain accurate photometry for many of the RSG candidates in the catalog of Nakamura et al. (2016). However, more work needs to be done exploring the short exposures and calibrating them correctly in order to obtain useful, accurate photometry, which will be an active avenue of research for the PGIR team in the future. Furthermore, understanding the heating effects of the detector will also be an active area of research for the team, as being able to resolve this issue will allow for the short exposures to use an even smaller amount of frame times. This would increase the dynamic range of PGIR to even lower magnitudes, allowing for the study of the very brightest sources in and near our galaxy.

Understanding the progenitors of CCSNe, and obtaining their photometric data right before they collapse and explode is an incredibly important avenue to be pursued in future CCSNe studies that PGIR is making huge advances in. The future of NIR time-domain astronomy is incredibly exciting, and this thesis is just one small example of the amazing work that can be done through uncovering the mysteries of the near-infrared sky.

BIBLIOGRAPHY

Björnsson, Claes-Ingvar and Claes Fransson (Apr. 2004). "The X-Ray and Radio Emission from SN 2002ap: The Importance of Compton Scattering". In: 605.2, pp. 823–829. DOI: 10.1086/382584. arXiv: astro-ph/0401196 [astro-ph].

Blagorodnova, Nadejda et al. (Feb. 2018). "The SED Machine: A Robotic Spectrograph for Fast Transient Classification". In: *Publications of the Astronomical Society of the Pacific* 130.985, p. 035003. DOI: 10.1088/1538-3873/aaa53f. URL: https://doi.org/10.1088%2F1538-3873%2Faaa53f.

Branch, David and J. Craig Wheeler (2017). *Supernova Explosions*. DOI: 10.1007/978-3-662-55054-0.

Breeveld, A. A. et al. (Aug. 2011). "An Updated Ultraviolet Calibration for the Swift/UVOT". In: *American Institute of Physics Conference Series*. Ed. by J. E. McEnery, J. L. Racusin, and N. Gehrels. Vol. 1358. American Institute of Physics Conference Series, pp. 373–376. DOI: 10.1063/1.3621807. arXiv: 1102.4717 [astro-ph.IM].

Burrows, David N. et al. (Oct. 2005). "The Swift X-Ray Telescope". In: 120.3-4, pp. 165–195. DOI: 10.1007/s11214-005-5097-2. arXiv: astro-ph/0508071 [astro-ph].

Chevalier, R. A. (Aug. 1982). "The radio and X-ray emission from type II supernovae." In: 259, pp. 302–310. DOI: 10.1086/160167.

Chevalier, Roger A. (May 1998). "Synchrotron Self-Absorption in Radio Supernovae". In: 499.2, pp. 810–819. DOI: 10.1086/305676.

Chevalier, Roger A. and Claes Fransson (Nov. 2006). "Circumstellar Emission from Type Ib and Ic Supernovae". In: 651.1, pp. 381–391. DOI: 10.1086/507606. arXiv: astro-ph/0607196 [astro-ph].

De, K., M. Hankins, M. Kasliwal, et al. (Feb. 2020). "Palomar Gattini-IR: Survey Overview, Data Processing System, On-sky Performance and First Results". In: 132, p. 025001. DOI: 10.1088/1538-3873/ab6069. arXiv: 1910.13319 [astro-ph].

De, K., M. Hankins, M. M. Kasliwal, et al. (July 2020). "Palomar Gattini-IR NIR discovery of a candidate young supernova PGIR20eid / AT2020qmp in UGC07125 at 12 Mpc". In: *The Astronomer's Telegram* 13909, p. 1.

De, Kishalay et al. (May 2021). "A Population of Heavily Reddened, Optically Missed Novae from Palomar Gattini-IR: Constraints on the Galactic Nova Rate". In: 912.1, 19, p. 19. DOI: 10.3847/1538-4357/abeb75. arXiv: 2101.04045 [astro-ph.HE].

de Vaucouleurs, Gerard et al. (1991). *Third Reference Catalogue of Bright Galaxies*.

Dessart, Luc, Eli Livne, and Roni Waldman (Oct. 2010). "Determining the main-sequence mass of Type II supernova progenitors". In: 408.2, pp. 827–840. DOI: 10.1111/j.1365-2966.2010.17190.x. arXiv: 1006.2268 [astro-ph.SR].

Dong, Yize et al. (Jan. 2020). "Supernova 2018cuf: A Type IIP Supernova with a Slow Fall from Plateau". In: 906.1, 56, p. 56. DOI: 10.3847/1538-4357/abc417. arXiv: 2010.09764 [astro-ph.HE].

Evans, P. A., A. P. Beardmore, K. L. Page, J. P. Osborne, et al. (Aug. 2009). "Methods and results of an automatic analysis of a complete sample of Swift-XRT observations of GRBs". In: 397.3, pp. 1177–1201. DOI: 10.1111/j.1365-2966.2009.14913.x. arXiv: 0812.3662 [astro-ph].

Evans, P. A., A. P. Beardmore, K. L. Page, L. G. Tyler, et al. (July 2007). "An online repository of Swift/XRT light curves of γ-ray bursts". In: 469.1, pp. 379–385. DOI: 10.1051/0004-6361:20077530. arXiv: 0704.0128 [astro-ph].

Filippenko, Alexei V. (1997). "OPTICAL SPECTRA OF SUPERNOVAE". In: *Annual Review of Astronomy and Astrophysics* 35.1, pp. 309–355. DOI: 10.1146/annurev.astro.35.1.309. eprint: https://doi.org/10.1146/annurev.astro.35.1.309. URL: https://doi.org/10.1146/annurev.astro.35.1.309.

Frostig, Danielle et al. (Dec. 2020). "Design requirements for the Wide-field Infrared Transient Explorer (WINTER)". In: *Society of Photo-Optical Instrumentation Engineers (SPIE) Conference Series*. Vol. 11447. Society of Photo-Optical Instrumentation Engineers (SPIE) Conference Series, p. 1144767. DOI: 10.1117/12.2562842. arXiv: 2105.01219 [astro-ph.IM].

Fryer, Chris L. and Vassiliki Kalogera (June 2001). "Theoretical Black Hole Mass Distributions". In: 554.1, pp. 548–560. DOI: 10.1086/321359. arXiv: astro-ph/9911312 [astro-ph].

Gal-Yam, Avishay (2017). "Observational and Physical Classification of Supernovae". In: *Handbook of Supernovae*. Ed. by Athem W. Alsabti and Paul Murdin. Cham: Springer International Publishing, pp. 195–237. ISBN: 978-3-319-21846-5. DOI: 10.1007/978-3-319-21846-5_35. URL: https://doi.org/10.1007/978-3-319-21846-5_35.

Gehrels, N. et al. (Aug. 2004). "TheSwiftGamma-Ray Burst Mission". In: *The Astrophysical Journal* 611.2, pp. 1005–1020. DOI: 10.1086/422091. URL: https://doi.org/10.1086%2F422091.

Goldberg, Jared A., Lars Bildsten, and Bill Paxton (July 2019). "Inferring Explosion Properties from Type II-Plateau Supernova Light Curves". In: 879.1, 3, p. 3. DOI: 10.3847/1538-4357/ab22b6. arXiv: 1903.09114 [astro-ph.SR].

Grossan, Bruce et al. (Aug. 1999). "An Infrared Search for Extinguished Supernovae in Starburst Galaxies". In: 118.2, pp. 705–718. DOI: 10.1086/300962. arXiv: astro-ph/9812253 [astro-ph].

Guillochon, James et al. (Jan. 2017). "An Open Catalog for Supernova Data". In: 835.1, 64, p. 64. DOI: 10.3847/1538-4357/835/1/64. arXiv: 1605.01054 [astro-ph.SR].

Herter, Terry L. et al. (July 2008). "The performance of TripleSpec at Palomar". In: *Ground-based and Airborne Instrumentation for Astronomy II*. Ed. by Ian S. McLean and Mark M. Casali. Vol. 7014. Society of Photo-Optical Instrumentation Engineers (SPIE) Conference Series, p. 70140X. DOI: 10.1117/12.789660.

HI4PI Collaboration et al. (Oct. 2016). "HI4PI: A full-sky H I survey based on EBHIS and GASS". In: 594, A116, A116. DOI: 10.1051/0004-6361/201629178. arXiv: 1610.06175 [astro-ph.GA].

Horesh, Assaf, Itai Sfaradi, et al. (Nov. 2020). "A Non-equipartition Shock Wave Traveling in a Dense Circumstellar Environment around SN 2020oi". In: 903.2, 132, p. 132. DOI: 10.3847/1538-4357/abbd38. arXiv: 2006.13952 [astro-ph.HE].

Horesh, Assaf, Christopher Stockdale, et al. (Dec. 2013a). "An early and comprehensive millimetre and centimetre wave and X-ray study of SN 2011dh: a non-equipartition blast wave expanding into a massive stellar wind". In: 436.2, pp. 1258–1267. DOI: 10.1093/mnras/stt1645. arXiv: 1209.1102 [astro-ph.CO].

– (Dec. 2013b). "An early and comprehensive millimetre and centimetre wave and X-ray study of SN 2011dh: a non-equipartition blast wave expanding into a massive stellar wind". In: 436.2, pp. 1258–1267. DOI: 10.1093/mnras/stt1645. arXiv: 1209.1102 [astro-ph.CO].

Jayasinghe, T. et al. (June 2021). "A unicorn in monoceros: the $3\,\mathrm{M}_\odot$ dark companion to the bright, nearby red giant V723 Mon is a non-interacting, mass-gap black hole candidate". In: 504.2, pp. 2577–2602. DOI: 10.1093/mnras/stab907. arXiv: 2101.02212 [astro-ph.SR].

Jencson, Jacob E. et al. (Nov. 2019). "The SPIRITS Sample of Luminous Infrared Transients: Uncovering Hidden Supernovae and Dusty Stellar Outbursts in Nearby Galaxies". In: 886.1, 40, p. 40. DOI: 10.3847/1538-4357/ab4a01. arXiv: 1901.00871 [astro-ph.HE].

Jerkstrand, A., C. Fransson, et al. (Oct. 2012). "The progenitor mass of the Type IIP supernova SN 2004et from late-time spectral modeling". In: 546, A28, A28. DOI: 10.1051/0004-6361/201219528. arXiv: 1208.2183 [astro-ph.HE].

Jerkstrand, A., S. J. Smartt, et al. (Apr. 2014). "The nebular spectra of SN 2012aw and constraints on stellar nucleosynthesis from oxygen emission lines". In: 439.4, pp. 3694–3703. DOI: 10.1093/mnras/stu221. arXiv: 1311.2031 [astro-ph.SR].

Jerkstrand, Anders (Dec. 2011). "Spectral modeling of nebular-phase supernovae". PhD thesis. -.

Jerram, Paul and James Beletic (2019). "Teledyne's high performance infrared detectors for Space missions". In: *International Conference on Space Optics — ICSO 2018*. Ed. by Zoran Sodnik, Nikos Karafolas, and Bruno Cugny. Vol. 11180. International Society for Optics and Photonics. SPIE, pp. 1270–1279. DOI: 10.1117/12.2536040. URL: https://doi.org/10.1117/12.2536040.

Kaiser, Nicholas et al. (Dec. 2002). "Pan-STARRS: A Large Synoptic Survey Telescope Array". In: *Survey and Other Telescope Technologies and Discoveries*. Ed. by J. Anthony Tyson and Sidney Wolff. Vol. 4836. Society of Photo-Optical Instrumentation Engineers (SPIE) Conference Series, pp. 154–164. DOI: 10.1117/12.457365.

Kasliwal, Mansi M. et al. (Apr. 2017). "SPIRITS: Uncovering Unusual Infrared Transients with Spitzer". In: 839.2, 88, p. 88. DOI: 10.3847/1538-4357/aa6978. arXiv: 1701.01151 [astro-ph.HE].

Krisciunas, Kevin et al. (Jan. 2009). "Do the Photometric Colors of Type II-P Supernovae Allow Accurate Determination of Host Galaxy Extinction?" In: 137.1, pp. 34–41. DOI: 10.1088/0004-6256/137/1/34. arXiv: 0809.2591 [astro-ph].

Lourie, Nathan P. et al. (Dec. 2020). "The wide-field infrared transient explorer (WINTER)". In: *Society of Photo-Optical Instrumentation Engineers (SPIE) Conference Series*. Vol. 11447. Society of Photo-Optical Instrumentation Engineers (SPIE) Conference Series, 114479K. DOI: 10.1117/12.2561210. arXiv: 2102.01109 [astro-ph.IM].

Maiolino, R. et al. (July 2002). "Discovery of two infrared supernovae: A new window on the SN search". In: 389, pp. 84–92. DOI: 10.1051/0004-6361:20020604. arXiv: astro-ph/0204107 [astro-ph].

Martin, Emily C. et al. (Aug. 2018). "An overview of the NIRSPEC upgrade for the Keck II telescope". In: *Ground-based and Airborne Instrumentation for Astronomy VII*. Ed. by Christopher J. Evans, Luc Simard, and Hideki Takami. Vol. 10702. Society of Photo-Optical Instrumentation Engineers (SPIE) Conference Series, 107020A. DOI: 10.1117/12.2312266. arXiv: 1808.06024 [astro-ph.IM].

Martinez, Laureano and Melina C. Bersten (Sept. 2019). "Mass discrepancy analysis for a select sample of Type II-Plateau supernovae". In: 629, A124, A124. DOI: 10.1051/0004-6361/201834818. arXiv: 1908.01828 [astro-ph.SR].

Masci, Frank J. et al. (Dec. 2018). "The Zwicky Transient Facility: Data Processing, Products, and Archive". In: *Publications of the Astronomical Society of the Pacific* 131.995, p. 018003. ISSN: 1538-3873. DOI: 10.1088/1538-3873/aae8ac. URL: http://dx.doi.org/10.1088/1538-3873/aae8ac.

Mattila, S. et al. (Aug. 2012). "CORE-COLLAPSE SUPERNOVAE MISSED BY OPTICAL SURVEYS". In: *The Astrophysical Journal* 756.2, p. 111. DOI: 10.1088/0004-637x/756/2/111. URL: https://doi.org/10.1088/0004-637x/756/2/111.

Moore, A. and M. Kasliwal (Jan. 2019). "Palomar Gattini-IR: Survey Overview, Data Processing System, On-sky Performance and First Results". In: *Nature Astronomy* 3, p. 109. DOI: 10.1038/s41550-018-0675-x. arXiv: 1910.13319 [astro-ph].

Morozova, Viktoriya, Anthony L. Piro, Mathieu Renzo, et al. (Nov. 2015). "Light Curves of Core-collapse Supernovae with Substantial Mass Loss Using the New Open-source SuperNova Explosion Code (SNEC)". In: 814.1, 63, p. 63. DOI: 10.1088/0004-637X/814/1/63. arXiv: 1505.06746 [astro-ph.HE].

Morozova, Viktoriya, Anthony L. Piro, and Stefano Valenti (Mar. 2017). "Unifying Type II Supernova Light Curves with Dense Circumstellar Material". In: 838.1, 28, p. 28. DOI: 10.3847/1538-4357/aa6251. arXiv: 1610.08054 [astro-ph.HE].

– (May 2018). "Measuring the Progenitor Masses and Dense Circumstellar Material of Type II Supernovae". In: 858.1, 15, p. 15. DOI: 10.3847/1538-4357/aab9a6. arXiv: 1709.04928 [astro-ph.HE].

Nagao, Takashi, Keiichi Maeda, and Masaomi Tanaka (Oct. 2017). "Circumstellar Light Echo as a Possible Origin of the Polarization of Type IIP Supernovae". In: 847.2, 111, p. 111. DOI: 10.3847/1538-4357/aa8b0d. arXiv: 1709.02077 [astro-ph.HE].

– (July 2018). "Multi-band Polarization of Type IIP Supernovae Due to Light Echo from Circumstellar Dust". In: 861.1, 1, p. 1. DOI: 10.3847/1538-4357/aac94e. arXiv: 1805.11865 [astro-ph.HE].

Nakamura, Ko et al. (Sept. 2016). "Multimessenger signals of long-term core-collapse supernova simulations: synergetic observation strategies". In: 461.3, pp. 3296–3313. DOI: 10.1093/mnras/stw1453. arXiv: 1602.03028 [astro-ph.HE].

Oke, J. B., J. G. Cohen, et al. (Apr. 1995). "The Keck Low-Resolution Imaging Spectrometer". In: 107, p. 375. DOI: 10.1086/133562.

Oke, J. B. and J. E. Gunn (June 1982). "An Efficient Low Resolution and Moderate Resolution Spectrograph for the Hale Telescope". In: *Publications of the Astronomical Society of the Pacific* 94, p. 586. DOI: 10.1086/131027. URL: https://doi.org/10.1086%2F131027.

Özel, Feryal et al. (Dec. 2010). "THE BLACK HOLE MASS DISTRIBUTION IN THE GALAXY". In: *The Astrophysical Journal* 725.2, pp. 1918–1927. DOI: 10.1088/0004-637x/725/2/1918. URL: https://doi.org/10.1088/0004-637x/725/2/1918.

Rabinak, Itay and Eli Waxman (Jan. 2011). "THE EARLY UV/OPTICAL EMISSION FROM CORE-COLLAPSE SUPERNOVAE". In: *The Astrophysical Journal* 728.1, p. 63. DOI: 10.1088/0004-637x/728/1/63. URL: https://doi.org/10.1088/0004-637x/728/1/63.

Richardson, Dean et al. (May 2014). "Absolute-magnitude Distributions of Supernovae". In: 147.5, 118, p. 118. DOI: 10.1088/0004-6256/147/5/118. arXiv: 1403.5755 [astro-ph.SR].

Roming, Peter W. A. et al. (Oct. 2005). "The Swift Ultra-Violet/Optical Telescope". In: 120.3-4, pp. 95–142. DOI: 10.1007/s11214-005-5095-4. arXiv: astro-ph/0507413 [astro-ph].

Sapir, Nir and Eli Waxman (Apr. 2017). "UV/Optical Emission from the Expanding Envelopes of Type II Supernovae". In: *The Astrophysical Journal* 838.2, p. 130. DOI: 10.3847/1538-4357/aa64df. URL: https://doi.org/10.3847/1538-4357/aa64df.

Schlafly, Edward F. and Douglas P. Finkbeiner (Aug. 2011). "Measuring Reddening with Sloan Digital Sky Survey Stellar Spectra and Recalibrating SFD". In: 737.2, 103, p. 103. DOI: 10.1088/0004-637X/737/2/103. arXiv: 1012.4804 [astro-ph.GA].

Simcoe, Robert A. et al. (Feb. 2019). "Background-limited Imaging in the Near Infrared with Warm InGaAs Sensors: Applications for Time-domain Astronomy". In: 157.2, 46, p. 46. DOI: 10.3847/1538-3881/aae094. arXiv: 1805.08791 [astro-ph.IM].

Sivanandam, Suresh et al. (2018). "Gemini infrared multi-object spectrograph: instrument overview". In: *Ground-based and Airborne Instrumentation for Astronomy VII*. Ed. by Christopher J. Evans, Luc Simard, and Hideki Takami. Vol. 10702. International Society for Optics and Photonics. SPIE, pp. 456–467. DOI: 10.1117/12.2313924. URL: https://doi.org/10.1117/12.2313924.

Smartt, S. J. (Apr. 2015). "Observational Constraints on the Progenitors of Core-Collapse Supernovae: The Case for Missing High-Mass Stars". In: 32, e016, e016. DOI: 10.1017/pasa.2015.17. arXiv: 1504.02635 [astro-ph.SR].

Smartt, Stephen J. (2009). "Progenitors of Core-Collapse Supernovae". In: *Annual Review of Astronomy and Astrophysics* 47.1, pp. 63–106. DOI: 10.1146/annurev-astro-082708-101737. eprint: https://doi.org/10.1146/annurev-astro-082708-101737. URL: https://doi.org/10.1146/annurev-astro-082708-101737.

Soderberg, A. M. et al. (June 2012). "Panchromatic Observations of SN 2011dh Point to a Compact Progenitor Star". In: 752.2, 78, p. 78. DOI: 10.1088/0004-637X/752/2/78. arXiv: 1107.1876 [astro-ph.HE].

Sukhbold, Tuguldur et al. (Apr. 2016). "Core-collapse Supernovae from 9 to 120 Solar Masses Based on Neutrino-powered Explosions". In: 821.1, 38, p. 38. DOI: 10.3847/0004-637X/821/1/38. arXiv: 1510.04643 [astro-ph.HE].

Tinyanont, Samaporn, Maxwell Millar-Blanchaer, et al. (Sept. 2019). "Achieving a spectropolarimetric precision better than 0.1% in the near-infrared with WIRC+Pol". In: *Polarization Science and Remote Sensing IX*. Vol. 11132. So-

ciety of Photo-Optical Instrumentation Engineers (SPIE) Conference Series, p. 1113209. DOI: 10.1117/12.2529863. arXiv: 1908.10409 [astro-ph.IM].

Tinyanont, Samaporn, Maxwell A. Millar-Blanchaer, et al. (Feb. 2019a). "WIRC+Pol: A Low-resolution Near-infrared Spectropolarimeter". In: 131.996, p. 025001. DOI: 10.1088/1538-3873/aaef0f. arXiv: 1811.03138 [astro-ph.IM].

– (Feb. 2019b). "WIRC+Pol: A Low-resolution Near-infrared Spectropolarimeter". In: 131.996, p. 025001. DOI: 10.1088/1538-3873/aaef0f. arXiv: 1811.03138 [astro-ph.IM].

Tomasella, L. et al. (Oct. 2014). "Asiago Supernova classification program: Blowing out the first two hundred candles". In: *Astronomische Nachrichten* 335.8, p. 841. DOI: 10.1002/asna.201412068. arXiv: 1403.7233 [astro-ph.HE].

Tully, R. Brent, Hélène M. Courtois, and Jenny G. Sorce (Aug. 2016). "Cosmicflows-3". In: 152.2, 50, p. 50. DOI: 10.3847/0004-6256/152/2/50. arXiv: 1605.01765 [astro-ph.CO].

Uomoto, Alan (Nov. 1986). "What Stars Become Peculiar Type I Supernovae?" In: 310, p. L35. DOI: 10.1086/184777.

Utrobin, V. P. and N. N. Chugai (Nov. 2009). "High mass of the type IIP supernova 2004et inferred from hydrodynamic modeling". In: 506.2, pp. 829–834. DOI: 10.1051/0004-6361/200912273. arXiv: 0908.2403 [astro-ph.SR].

– (Mar. 2015). "Parameters of type IIP SN 2012A and clumpiness effects". In: 575, A100, A100. DOI: 10.1051/0004-6361/201424822. arXiv: 1411.6480 [astro-ph.SR].

– (Dec. 2017). "Luminous Type IIP SN 2013ej with high-velocity ^{56}Ni ejecta". In: 472.4, pp. 5004–5010. DOI: 10.1093/mnras/stx2415. arXiv: 1709.05573 [astro-ph.HE].

Voshchinnikov, N. V. (Dec. 2012). "Interstellar extinction and interstellar polarization: Old and new models". In: 113.18, pp. 2334–2350. DOI: 10.1016/j.jqsrt.2012.06.013. arXiv: 1206.4090 [astro-ph.GA].

Wang, L. and J. C. Wheeler (Sept. 2008). "Spectropolarimetry of supernovae." In: 46, pp. 433–474. DOI: 10.1146/annurev.astro.46.060407.145139. arXiv: 0811.1054 [astro-ph].

Woosley, S. E. and A. Heger (Apr. 2007). "Nucleosynthesis and remnants in massive stars of solar metallicity". In: 442.1-6, pp. 269–283. DOI: 10.1016/j.physrep.2007.02.009. arXiv: astro-ph/0702176 [astro-ph].

Yadav, Naveen et al. (Feb. 2014). "Electron Cooling in a Young Radio Supernova: SN 2012aw". In: 782.1, 30, p. 30. DOI: 10.1088/0004-637X/782/1/30. arXiv: 1311.3568 [astro-ph.HE].